PUCRS

SCHOOL OF TECHNOLOGY

GRADUATE PROGRAM IN ELECTRICAL ENGINEERING

MASTER DEGREE IN ELECTRICAL ENGINEERING

EDUARDO SCHEFFER SARAIVA

CONTROL DESIGN FOR ROBOTIC MANIPULATOR SYSTEMS SUBJECT TO SATURATING ACTUATORS

Porto Alegre

2019

PÓS-GRADUAÇÃO - *STRICTO SENSU*

Pontifícia Universidade Católica
do Rio Grande do Sul

EDUARDO SCHEFFER SARAIVA

CONTROL DESIGN FOR ROBOTIC MANIPULATOR SYSTEMS SUBJECT TO SATURATING ACTUATORS

Dissertation presented for the Graduate Program in Electrical Engineering at the Pontifical Catholic University of Rio Grande do Sul, as requirement for the Degree of Master in Electrical Engineering.

Supervisor: Rafael da Silveira Castro
Co-supervisor: Aurélio Tergolina Salton

Porto Alegre
2019

Ficha Catalográfica

S243c Saraiva, Eduardo Scheffer

Control Design for Robotic Manipulator Systems Subject to Saturating Actuators / Eduardo Scheffer Saraiva . – 2019.
77 p.
Dissertação (Mestrado) – Programa de Pós-Graduação em Engenharia Elétrica, PUCRS.

Orientador: Prof. Dr. Rafael da Silveira Castro.
Co-orientador: Prof. Dr. Aurélio Tergolina Salton.

1. Quaternions. 2. Differential Algebraic Representation. 3. Linear Matrix Inequalities. 4. Input Saturation. 5. Robotic Manipulator. I. Castro, Rafael da Silveira. II. Salton, Aurélio Tergolina. III. Título.

Elaborada pelo Sistema de Geração Automática de Ficha Catalográfica da PUCRS
com os dados fornecidos pelo(a) autor(a).
Bibliotecária responsável: Clarissa Jesinska Selbach CRB-10/2051

Pontifícia Universidade Católica do Rio Grande do Sul
ESCOLA POLITÉCNICA
PROGRAMA DE PÓS-GRADUAÇÃO EM ENGENHARIA ELÉTRICA - PPGEE

CONTROL DESIGN FOR ROBOTIC MANIPULATOR SYSTEMS SUBJECT TO SATURATING ACTUATORS

CANDIDATO: EDUARDO SCHEFFER SARAIVA

Esta Dissertação de Mestrado foi julgada para obtenção do título de MESTRE EM ENGENHARIA ELÉTRICA e aprovada em sua forma final pelo Programa de Pós-Graduação em Engenharia Elétrica da Pontifícia Universidade Católica do Rio Grande do Sul.

DR. RAFAEL DA SILVEIRA CASTRO - ORIENTADOR

DR. AURELIO TERGOLINA SALTON - COORIENTADOR

BANCA EXAMINADORA

DR. DIEGO ECKHARD - UFRGS

DR. LUCIANO GONÇALVES MOREIRA - IFSUL

DR. GUILHERME ARAUJO PIMENTEL - PPGEE - PUCRS

PUCRS
Av. Ipiranga, 6681 - Predio 32 - Sala 507 | CEP 90619-900 | Porto Alegre, RS - Brasil
Fone: (51) 3320-3540 | E-mail: engenharia.pg.eletrica@pucrs.br | www.pucrs.br/politecnica

Acknowledgements

This study was partially supported by CAPES and CNPq Brazil under grant 306214/2018-0, in cooperation with Hewlett-Packard Brazil Ltda using incentives of Brazilian Informatics Law (Law nº 8.2.48 of 1991).

Abstract

This Dissertation proposes a systematic control design procedure for planar robotic manipulator systems via semidefinite programming. The fundamental idea is to represent the body orientation in terms of quaternions and to express the system equations of motion in the differential-algebraic representation. This approach allows us to synthesize a state feedback controller by a convex optimization problem subject to Linear Matrix Inequalities, in order to ensure the closed-loop asymptotic and exponential stability. This method is able to provide rigorous theoretical guarantees considering the nonlinear dynamics involved in a robotic manipulator system, without resorting to any kind of linearization or approximation. Furthermore, the proposed framework, which is based on linear matrix inequalities, is highly versatile for extensions. To demonstrate this point, this Dissertation also addresses the control input saturation in the control design. Numerical examples of the nonlinear 2-link robotic manipulator with and without input saturation are provided to illustrate our proposed method.

Key-words: Quaternions, Differential Algebraic Representation, Linear Matrix Inequalities, Input Saturation, Robotic Manipulator, Newton-Euler Algorithm.

Resumo

Esta Dissertação propõe uma síntese sistemática do controlador considerando as não linearidades de um manipulador robótico planar através de otimização semidefinida. A ideia fundamental é representar a orientação do corpo em termos de quatérnions e acomodar o sistema numa representação algébrico-diferencial. Esta abordagem permite analisar e sintetizar o controlador assumindo um problema de otimização convexo sujeito a desigualdades matriciais lineares, a fim de garantir a estabilidade assintótica e exponencial de malha fechada. Neste método, nenhuma linearização é necessária e a adição de condições extras ao projeto de controle torna-se mais simples. Este método é capaz de fornecer garantias teóricas rigorosas considerando a dinâmica não linear envolvida em um sistema de manipulador robótico, sem recorrer a qualquer tipo de linearização ou aproximação. Além disso, o framework proposto, que é baseado em desigualdades matriciais lineares, é altamente versátil para extensões. Para demonstrar este ponto, esta Dissertação também aborda a saturação de entrada no projeto de controle. Exemplos numéricos do manipulador robótico não-linear de 2 elos com e sem saturação de entrada são fornecidos para ilustrar o método proposto.

Palavras-chaves: Quatérnions, Representação Diferencial-Algébrica, Desigualdade Matriciais Lineares, Saturação de Entrada, Manipuladores Robóticos, Algoritmo Newton-Euler.

List of Figures

List of Tables

List of abbreviations and acronyms

DAR	Differential-Algebraic Representation
LMI	Linear Matrix Inequality

List of symbols

$\dot{x}$	time derivative $\mathrm{d}x/\mathrm{d}t$
$\ddot{x}$	second order time derivative $\mathrm{d}^2x/\mathrm{d}t^2$
$\|\|x\|\|$	euclidean norm $\sqrt{x^\intercal x}$
x_i	i-th element of vector x
$A_{[i]}$	i-th row of matrix A
$A_{[i,j]}$	term located at the i-th row and j-th column of matrix A
I	identity matrix
$A^\intercal$	transpose of matrix A
A^{-1}	inverse of matrix A
$\mathrm{tr}(A)$	trace of matrix A
$\mathrm{He}\{A\}$	symmetric block $A + A^\intercal$
$\mathrm{diag}\{A, B\}$	block diagonal matrix formed with A and B
$A \succ 0$	matrix A is positive-definite
$A \prec 0$	matrix A is negative-definite
$(\star)$	symmetric elements in a matrix
$\mathbb{N}$	set of natural numbers
$\mathbb{R}$	set of real numbers
$\mathbb{R}^n$	set of real-valued vectors with n elements
$\mathbb{R}^{n\times m}$	set of real-valued matrices with n rows and m columns
$\mathcal{V}\{\mathcal{X}\}$	set of vertices of a polytope $\mathcal{X}$
$a \times b$	cross product between the vectors a and b

Contents

1 Introduction

Robotic manipulators have been widely studied in control engineering in various areas, for example manufacturing (CHERUBINI et al., 2016; RUS; TOLLEY, 2015), medical applications (TAYLOR et al., 2016; BURGNER-KAHRS; RUCKER; CHOSET, 2015) and devices for search and rescue (WU et al., 2017). In practice, manipulator control design is a particularly difficult task due to the multivariable nonlinear nature of its model (SPONG et al., 2006; SICILIANO; KHATIB, 2016), and physical limitation of the actuators, such as input saturation. All these intrinsic characteristics require a robust and systematic control design methodologies. Even though, according to the International Federation of Robotics, more than 3 million industrial robots will be in use in factories around the world by 2020 (IFR, 2017). As a result, considerable attention has been given to the design of practical controllers that are simple to implement and give optimally controller performance (BELOV; KHOA; TRUONG, 2019), (GENG; ARAKELIAN, 2019).

In the literature, many nonlinear control techniques in this context can be found, such as Passivity-based control (WALSH; FORBES, 2015) where an extension of the Lyapunov function is presented by using the system energy. Sliding mode techniques were used in KALI (2015b), ZHANG XUZHI LAI (2019) where a discontinuous control signal is applied. Based on the inverse dynamic method and using the feedback linearization, a model-based controller was designed in KALI (2015a). Also techniques such as robust H_∞ control (COSTA FABIAN A. LARA-MOLINA, 2018) where the uncertainties of the manipulator were considered for the trajectory tracking, the implementation of the robustified predictive controller in real-time is presented in LARA-MOLINA et al. (2014), a robust Neural Network controller has been designed for the control of robotic manipulators in the presence of external disturbances that were studied in RAHMANI; BELKHEIRI (2016). Likewise, many evolutionary algorithms (ZHANG XUZHI LAI , 2018) presents a position control strategy based on the differential evolution algorithm. A two-stage control strategy based on the hybrid intelligent optimization algorithm is studied in WANGA XUZHI LAI (2017), the fuzzy PD control strategy were studied in (CHEN, 2018; GUSNGZHENG WANG XUESONG, 2002). Most of the aforementioned studies considers the knowledge of the real model or the operation of the manipulator in a local region considering linearization methods in open or closed-loop, or techniques that do not provide closed-loop asymptotic stability guarantees.

Efforts to represent the system in a way that the powerful control methods based on convex optimization can be applied are increasingly in importance. A well-established theory for control design considering nonlinear systems is the differential-algebraic representation (TROFINO, 2000; TROFINO; DEZUO, 2014), which consists in representing a nonlinear system by a differential equation combined with an algebraic equation. In this method all nonlin-

earities are lumped into a new vector variable subject to an algebraic constraint. COUTINHO et al. (2004) presents a method for stabilization of rational nonlinear systems, afterwards it was extended for systems subject to input saturation (COUTINHO; GOMES DA SILVA JR, 2007). Furthermore, TROFINO; DEZUO (2014) brought a complete overview of the differential-algebraic theory. Also important results based on output regulation are presented in CASTRO (2019). SALTON et al. (2017) uses the quaternion representation to cast a spacecraft model into the DAR format.

1.1 Contribution of the Dissertation

As shown in the previous section, state-of-the-art methods rely on well-behaved systems or linearization methods to use linear tools for controller design in the robotic manipulator context. Differently, this Dissertation proposes a solution able to systematically synthesize a state feedback controller, which considers the manipulator nonlinearities, that is, that does not make use of linearization methods and that provides formal guarantees such as the asymptotic stability of the closed-loop system. Moreover, the control design task is defined in terms of a convex optimization problem subject to Linear Matrix Inequality (LMI) constraints. To cast the nonlinear manipulator model in this framework, the model is primarily rewritten using the quaternion representation and expressed in the differential-algebraic representation (DAR). Taking advantage of the polynomial form of the nonlinearities given by the quaternion representation, the DAR is able to address systems with rational nonlinearities and it allows the characterization of a nonlinear control problem in terms of convex optimization. It is important to state that through this representation a collection of design tools, originally proposed for linear systems, may be applied to simplify and improve the controller design even though no linearization or any kind of approximation is employed. Once the system is in the DAR format the extra nonlinearities such as input saturation can be easily adressed in the analysis or problem design. Here lies the main contribution of the methodology, the mechanism rotations are primarily rewritten in quaternion form and the system dynamics are cast in a new differential algebraic representation with state-derivative components, allowing to easily deal with the system nonlinearities related to mechanical inertia effects.

1.2 Outline of the Text

The dissertation is organized as follows. Chapter 2 introduces the Newton-Euler approach to the robotic manipulator modeling and the theoretical background used throughout the work, such as Lyapunov stability and the LMI definition. Chapter 3 will describe the change of coordinates and the quaternion transformation of the system to be represented in the DAR format. In Chapter 4, the proposed controller design framework will be presented along with a numerical example illustrating the main theoretical results of the methodology. In Chapter 5,

the input saturation effect will be added to the controller design task, proving that extra constraints can be easily added to the optimization problem. Similarly to Chapter 4, this chapter ends with a numerical example showing a robotic manipulator simulation subject to saturating actuators. Finally, Chapter 6 will present final considerations about the dissertation and future work proposals.

2 Preliminaries

This chapter presents the main preliminary concepts of this dissertation. Section 2.1 shows the stability criteria of nonlinear systems in the Lyapunov sense. Afterwards, Section 2.2 presents an overview of some LMI based methods for stability analysis of nonlinear systems and control design. Section 2.5 shows the methodology used to develop the manipulator model. Section 2.6 introduces the Quaternion concept and its mathematical operations.

2.1 Stability of Nonlinear Systems

Consider an autonomous nonlinear system described by

$$\dot{x} = f(x)\ , \tag{1}$$

where $x \in \mathcal{X} \subseteq \mathbb{R}^n$ is the system state and $f : \mathcal{X} \to \mathbb{R}^n$ is a local Lipschitz map from $\mathcal{X}$ into $\mathbb{R}^n$. Suppose that the origin is an equilibrium point of (1), that is $f(0) = 0$. If the equilibirum point of (1) is not zero, it is always possible, without loss of generality, to shift the equilibrium point to the origin via a proper change of coordinates (KHALIL, 2002). Definition 2.1 formalizes the concepts of stability and asymptotic stability of an equilibrium point.

Definition 2.1. The origin of the system (1) is said to be:

- *stable* if, for each $\epsilon > 0$, there is some $l > 0$ such that

$$||x(0)|| < l \ \Rightarrow \ ||x(t)|| < \epsilon \ \forall\, t > 0\ ; \tag{2}$$

- *asymptotically stable* if it is stable and l can be chosen such that

$$||x(0)|| < l \ \Rightarrow \ \lim_{t\to\infty} ||x(t)|| = 0\ ; \tag{3}$$

- *unstable* if it is not stable.

Theorem 2.1 presents a fundamental Lyapunov result able to determine if the origin of system (1) is stable or asymptotically stable within some region.

Theorem 2.1. *Suppose that $x = 0$ is an equilibrium point of* (1) *in the domain given by $\mathcal{X} \subseteq \mathbb{R}^n$. Let $V : \mathcal{X} \to \mathbb{R}$ be a function such that*

$$V(0) = 0, V(x) > 0 \ \forall x \in \mathcal{X},\ x \neq 0, \tag{4}$$

$$\dot{V}(x) \leq 0 \ \forall x \in \mathcal{X}. \tag{5}$$

$$\mathcal{R} = \left\{ x \in \mathbb{R}^n : V(x) \leq \epsilon \right\} \subset \mathcal{X} \, , \tag{6}$$

Then the origin of the system (1) *is stable in* $\mathcal{R}$*. Furthermore, if*

$$\dot{V}(x) < 0 \ \textit{in} \ \mathcal{X} - \{0\}, \tag{7}$$

then the origin is asymptotically stable in $\mathcal{R}$*. Moreover, if* $\mathcal{X} = \mathbb{R}^n$ *and* $V(x)$ *is radially unbounded*[1]*, then the origin is globally asymptotically stable.*

Proof. See KHALIL (2002). □

Following the result presented by Theorem 2.1, it is possible to affirm that a set $\mathcal{R}$ for some $\epsilon > 0$, is said to be positively invariant with respect to system (1), i.e. all trajectories starting in $\mathcal{R}$ remain in $\mathcal{R}$. Also, region $\mathcal{R}$ is said to be a *domain of attraction estimate* (KHALIL, 2002) if condition (7) holds, meaning that all trajectories starting in $\mathcal{R}$ asymptotically approach the origin of system (1).

2.2 Linear Matrix Inequalities

A linear matrix inequality (LMI) is a particular type of constraint defined by the affine relation

$$F(x) = F_0 + \sum_{i=1}^{m} F_i x_i \succ 0, \tag{8}$$

where $x = \begin{bmatrix} x_1 & x_2 & \cdots & x_m \end{bmatrix}^\mathsf{T} \in \mathcal{R}^m$ is the vector of decision variables and $F_i \in \mathcal{R}^{n \times n} \, \forall i \in \{0, 1, \cdots, m\}$ are symmetric matrices. An important property of an LMI is the convexity of its correspondent set $\mathcal{F} = \{x \in \mathbb{R}^m : F(x) \succ 0\}$. Problems involving LMI constraints typically consists on minimizing a linear objective function $f(x) = c^\mathsf{T} x, c \in \mathcal{R}^m$, subject to $x \in \mathcal{F}$, i.e.:

$$\underset{x}{min} \ c^\mathsf{T} x \ \text{ s.t. } \ F(x) \succ 0, \tag{9}$$

which is a convex optimization problem.

In order to cast problems in the form of LMI constraints, some important lemmas are used in this work as presented below:

Lemma 2.1. *(Congruence transformation) Let* $P, Q \in \mathbb{R}^{n \times n}$ *be symmetric matrices such that* Q *is non-singular. Then*

$$P \succ 0 \quad \Leftrightarrow \quad Q \, P \, Q^\mathsf{T} \succ 0 \, . \tag{10}$$

[1] A function $V(x)$ is said to be radially unbounded if $V(x) \to \infty$ as $||x|| \to \infty$.

Lemma 2.2. *(Schur's complement) Consider matrices* $P = P^{\mathsf{T}} \in \mathbb{R}^{n\times n}$, $R \in \mathbb{R}^{n\times m}$ *and* $Q = Q^{\mathsf{T}} \in \mathbb{R}^{m\times m}$ *such that* $Q \succ 0$. *Then*

$$P - R\,Q^{-1}R^{\mathsf{T}} \succ 0 \quad \Leftrightarrow \quad \begin{bmatrix} P & R \\ R^{\mathsf{T}} & Q \end{bmatrix} \succ 0\,. \tag{11}$$

Lemma 2.3. *(Finsler's lemma) Consider matrices* $P = P^{\mathsf{T}} \in \mathbb{R}^{n\times n}$ *and* $R \in \mathbb{R}^{m\times n}$. *Then* $x^{\mathsf{T}}Px > 0\;\forall\, x \in \mathcal{L},\, x \neq 0$ *where*

$$\mathcal{L} = \left\{x \in \mathbb{R}^n : R\,x = 0\right\}, \tag{12}$$

if there exists a matrix $L \in \mathbb{R}^{n\times m}$ *such that*

$$P + \mathrm{He}\{LR\} \succ 0\,. \tag{13}$$

Lemma 2.4. *(S-Procedure) Consider symmetric matrices* $P_0, P_1, \ldots, P_m \in \mathbb{R}^{n\times n}$. *Then* $x^{\mathsf{T}}P_0\,x > 0\;\forall\, x \in \mathcal{Q},\, x \neq 0$ *where*

$$\mathcal{Q} = \left\{x \in \mathbb{R}^n : x^{\mathsf{T}}P_i\,x \leq 0\,,\; i = 1, 2, \ldots, m\right\}, \tag{14}$$

if there exist non-negative scalars $\tau_1, \tau_2, \ldots, \tau_m \in \mathbb{R}$ *such that*

$$P_0 + \sum_{i=1}^{m} \tau_i\,P_i \succ 0\,. \tag{15}$$

The proofs can be found in (BOYD et al., 1994).

2.3 Systems with Control Input Saturation

Consider a linear system with a state feedback control subject to input saturation:

$$\begin{cases} \dot{x} &= A\,x + B\,u \\ \mu &= K\,x \\ u &= \mathrm{sat}(\mu) \end{cases} \tag{16}$$

where $x \in \mathbb{R}^{n_x}$ is the system state, $u \in \mathbb{R}^{n_u}$ is the saturated control input and $\mu \in \mathbb{R}^{n_u}$ is the unsaturated control input. The nonlinear function $\mathrm{sat} : \mathbb{R}^{n_u} \to [-\overline{u}_1, \overline{u}_1] \times \ldots \times [-\overline{u}_{n_u}, \overline{u}_{n_u}]$ is defined as

$$\mathrm{sat}(\mu_j) \triangleq \begin{cases} \overline{u}_j & \text{if} \quad \mu_j \geq \overline{u}_j \\ -\overline{u}_j & \text{if} \quad \mu_j \leq -\overline{u}_j \\ \mu_j & \text{if} \quad \text{otherwise} \end{cases}. \tag{17}$$

A graphical depiction of function (17) is shown in Figure (1)

To solve the problem of designing a controller that asymptotically stabilizes the system (16), GOMES DA SILVA JR; TARBOURIECH(2005) proposed rewriting the saturation function as a deadzone type nonlinearity.

$$\varphi(\mu) \triangleq \mu - \mathrm{sat}(\mu)\,. \tag{18}$$

Figure 1 – Graphical depiction of the saturation function.

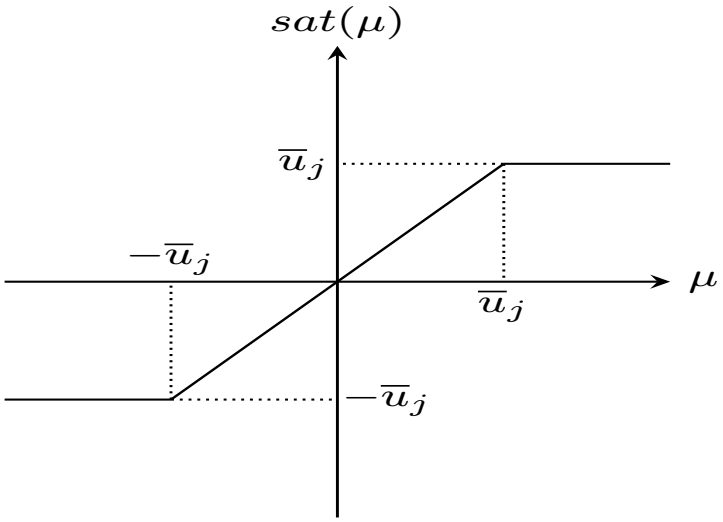

Adapted from: TARBOURIECH et al. (2011).

By introducing this definition, the gain K appears in the linear part of system (16) so that the closed-loop system can be written as

$$\dot{x} = \hat{A}\, x - B\, \varphi(Kx)\ , \tag{19}$$

where $\hat{A} \triangleq A + BK$. In order to deal with this deazone function $\varphi(\cdot)$, a generalized sector condition has also been proposed according to the following lemma, where the matrix G appears as an extra decision variable in the stability analysis or control design problem.

Lemma 2.5. *Consider vector functions $K, G : \mathbb{R}^{n_x} \to \mathbb{R}^{n_u}$. If $x \in \mathcal{S}$, where $\mathcal{S}$ is the polyhedral set*

$$\mathcal{S} = \left\{ x \in \mathbb{R}^{n_x} : |\, K_{[j]}x - G_{[j]}x \,| \,\leq\, \overline{u}_{[j]}\ ,\ j = 1, 2, \ldots, n_u \right\}\ , \tag{20}$$

then the following inequality is verified

$$\varphi^{\mathsf{T}}(Kx)\, T \Big(\varphi(Kx) - Gx \Big) \leq 0 \tag{21}$$

for any diagonal and positive-definite matrix $T \in \mathbb{R}^{n_u \times n_u}$.

Proof. Consider the three possible cases that follows:

(a) $-\overline{u}_{[j]} \leq K_{[j]}(x) \leq \overline{u}_{[j]}$. In this case, $\varphi(K_{[j]}(x)) = 0$ and then

$$\varphi^{\mathsf{T}}(K_{[j]}(x))\, T_{[j,j]} \Big(\varphi(K_{[j]}(x)) - G_{[j]}(x) \Big) = 0\ . \tag{22}$$

(b) $K_{[j]}(x) \geq \overline{u}_{[j]}$. In this case, $\varphi(K_{[j]}(x)) = K_{[j]}(x) - \overline{u}_{[j]} > 0$. If $x \in \mathcal{S}$, then $K_{[j]}(x) - G_{[j]}(x) \leq \overline{u}_{[j]}$, therefore it follows that $\varphi(K_{[j]}(x)) - G_{[j]}(x) \leq 0$. Consequently, one gets that

$$\varphi^{\mathsf{T}}(K_{[j]}(x))\, T_{[j,j]} \Big(\varphi(K_{[j]}(x)) - G_{[j]}(x) \Big) \leq 0\ . \tag{23}$$

(c) $K_{[j]}(x) \leq -\overline{u}_{[j]}$. In this case, $\varphi(K_{[j]}(x)) = K_{[j]}(x) + \overline{u}_{[j]} < 0$. If $x \in \mathcal{S}$, then $K_{[j]}(x) - G_{[j]}(x) \geq -\overline{u}_{[j]}$, therefore it follows that $\varphi(K_{[j]}(x)) - G_{[j]}(x) \geq 0$. Consequently, one also gets that (23).

From these three cases, provided that $x \in \mathcal{S}$ and that matrix T is diagonal and positive-definite, condition (21) is verified. □

Based on this lemma, theorems were developed for controller design (TARBOURIECH et al., 2011) where the S-procedure (Lemma 2.4) is employed in order to include the sector condition (21) into the Lypunov-based stability relations.

2.4 Rational Nonlinear Systems

The Differential-Algebraic Representation (DAR) makes use of an auxiliary vector $\xi(x)$ that groups nonlinear terms of degree equal or higher than two to represent rational systems. The DAR representation is given by,

$$\begin{aligned} \dot{x} &= A_1(x,\delta)x + A_2(x,\delta)\xi + B(x,\delta)u \\ 0 &= \Omega_1(x,\delta)x + \Omega_2(x,\delta)\xi + \Omega_3(x,\delta)u \end{aligned} \tag{24}$$

where $x \in \mathcal{X} \subseteq \mathbb{R}^{n_x}$ is the system state, $\xi : \mathcal{X} \to \mathbb{R}^{n_\xi}$ is a rational function and the matrices $A_1 : \mathcal{X} \to \mathbb{R}^{n_x \times n_x}$, $A_2 : \mathcal{X} \to \mathbb{R}^{n_x \times n_\xi}$, $\Omega_1 : \mathcal{X} \to \mathbb{R}^{n_\xi \times n_x}$, $\Omega_2 : \mathcal{X} \to \mathbb{R}^{n_\xi \times n_\xi}$ and $\Omega_3 : \mathcal{X} \to \mathbb{R}^{n_\xi \times n_u}$ are affine matrices with respect to x. Moreover, $\Omega_2(x)$ is supposedly non-singular inside $\mathcal{X}$, i.e. $\det\{\Omega_2(x)\} \neq 0 \; \forall \, x \in \mathcal{X}$. Every system originally described as (1), whose function $f(x)$ is a well-posed rational function[2] in $\mathcal{X}$, can be represented in the form of (24)[3] (TROFINO; DEZUO, 2014).

The analysis of the stability of nonlinear systems described by (24) is presented by TROFINO; DEZUO (2014) based on LMI constraints methods, providing a systematic approach to the controller design problem. Based on this, theorems were developed for controller design (TROFINO, 2000) where the Finsler's Lemma (Lemma 2.3) is used in order to address an equality restriction of DAR that will be further used in Chapter 4 and Chapter 5.

2.5 Newton-Euler Modeling

Robotic manipulators can be seen as a chain of links, each link being able to move relative to the other ones. In robotics, it is usual to use the Newton-Euler recursive algorithm

[2] A function $f(x)$ is said to be rational if it can be expressed as a fraction of polynomial functions and it is also well-posed in $\mathcal{X}$ if it has no singularities $\forall \, x \in \mathcal{X}$.

[3] It is important to state that this representation is not unique.

(SPONG et al., 2006), to describe the dynamics of the manipulator, which is composed of two parts the "Outward Iteration" and the "Inward Iteration". The outward iterations are responsible for computing the inertial forces acting in the links and the inward iterations responsible for computing the effective torque necessary to reach the forces obtained in the outward iteration.

Figure 2 – Two link planar manipulator

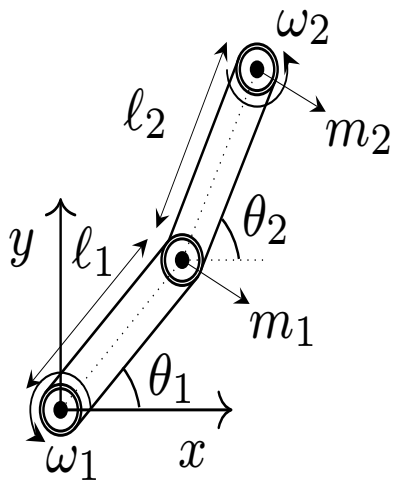

2.5.1 Outward Iteration

Considering the velocities propagation along the chain of a manipulator with rotational joints, the angular velocities of each link can be described as

$$\omega_{i+1} = R_{i+1}\,\omega_i + \dot{\theta}_{i+1}\,\hat{z}_{i+1}, \tag{25}$$

where $\omega_{i+1} \in \mathbb{R}^{3\times1}$ is the vector that contains the angular velocities of the link $i+1$ in relation to the reference frame, $R_{i+1} \in \mathbb{R}^{3\times3}$ is the rotation matrix that relates the link i to the link $i+1$, $\dot{\theta}_{i+1}$ is the link angular velocity in relation to the link frame, and $\hat{z} \in \mathbb{R}^{3\times1}$ is a auxiliary vector defining where the rotation $\dot{\theta}_i$ is being performed.

The linear velocity of the reference system $i+1$ is composed by the linear velocity and rotational velocity in relation to system i and can be obtained by the equation

$$v_{i+1} = R_{i+1}(v_i + \omega_i \times\ p_{i+1}), \tag{26}$$

where $v_{i+1} \in \mathbb{R}^3$ is the vector that contains the linear velocities of link $i+1$, $p_{i+1} \in \mathbb{R}^3$ is the distance of the center of mass of link i to the center of mass to the link $i+1$.

The angular acceleration is obtained by taking the derivative of equation (25)

$$\dot{\omega}_{i+1} = R_{i+1}\,\dot{\omega}_i + R_{i+1}\,\omega_i \times \dot{\theta}_{i+1}\,\hat{z}_{i+1} + \ddot{\theta}_{i+1}\,\hat{z}_{i+1}. \tag{27}$$

The linear acceleration of the system origin can be obtained by taking the derivative of equation (26)

$$\dot{v}_{i+1} = R_{i+1}[\omega_i \times p_{i+1} + \omega_i \times (\omega_i \times p_{i+1}) + \dot{v}_i]. \tag{28}$$

The linear acceleration of the body center of mass can be obtained by the following equation

$$\dot{v}_{C_i} = \dot{\omega}_i \times p_{C_i} + \omega_i \times (\omega_i + p_{C_i}) + \dot{v}_i. \tag{29}$$

Here it is necessary to use C_i as reference, which is a reference system with its origin located in the center of mass of each link and also has the same orientation of link i reference system.

In classical mechanics, the Newton-Euler equations describe the combination of the bodies orientation and translation. Traditionally, these equations are grouped in one single equation with six components through the use of matrices and vectors algebra. These laws relate the body center of mass with the sum of torques and forces acting on the system, such that the force f, acting in the body center of mass causing acceleration, is given by Newton's equation

$$f_i = m\dot{v}_{C_i}. \tag{30}$$

In a similar way, a rotating rigid body with angular velocity ω and angular acceleration $\dot{\omega}$, caused by a torque τ, is given by the Euler's equation:

$$\tau_i = J_{C_i}\dot{\omega} + \omega \times J_{C_i}\omega, \tag{31}$$

where J_{C_i} is the body inertia tensor described in relation to the center of mass located at the system origin C_i.

Once the accelerations have been computed, it is possible to calculate the forces acting in the center of mass of the links, by using equations (30) and (31) to each link.

2.5.2 Inward Iteration

After the inertial forces and accelerations have been computed, it is possible to compute the effective torque applied to each link that will lead to the forces computed in the Outward iteration. This can be done by using the balance of forces and balance of the momentum equation.

By adding the forces acting in the link i, the balance of forces can be written as

$$\hat{f}_i = R_{i+1}\ \hat{f}_{i+1} + f_i, \tag{32}$$

where $\hat{f}_i$ is the force actuating in the link i by the link $i-1$. Similarly by adding the torques around the center of mass of each link the following equation express the balance of momentum

$$\hat{n}_i = n_i + R_{i+1}\ \hat{n}_{i+1} + p_{C_i} \times f_i + p_{i+1} \times R_{i+1}\ \hat{f}_{i+1}, \tag{33}$$

where n_i is the torque exercised in the link i by the link $i-1$. Finally, the effective torque can be found by applying the $\hat{z}$ vector

$$\tau_i = \hat{n}_i^{\mathsf{T}}\ \hat{z}_i. \tag{34}$$

with τ denoting the effective torque that results in the torques presented in Newton-Euler equations. To synthesize the equations, the full algorithm is presented below:

Outward iterations: $i : 0 \to n$

$$\begin{aligned}
\omega_{i+1} &= R_{i+1}\omega_i + \dot{\theta}_{i+1}\ \hat{z}_{i+1} \\
\dot{\omega}_{i+1} &= R_{i+1}\ \dot{\omega}_i + R_{i+1}\ \omega_i \times \dot{\theta}_{i+1}\ \hat{z}_{i+1} + \ddot{\theta}_{i+1}\ \hat{z}_{i+1} \\
\dot{v}_{i+1} &= R_{i+1}[\omega_i \times p_{i+1} + \omega_i \times (\omega_i \times p_{i+1}) + \dot{v}_i] \\
\dot{v}_{C_{i+1}} &= \dot{\omega}_{i+1} \times p_{C_{i+1}} + \omega_{i+1} \times (\omega_{i+1} + p_{C_{i+1}}) + \dot{v}_{i+1} \\
f_{i+1} &= m_{i+1}\ \dot{v}_{C_{i+1}} \\
n_{i+1} &= J_{C_{i+1}}\ \dot{\omega}_{i+1} + \omega_{i+1} \times J_{C_{i+1}}\ {}^{i+1}\omega_{i+1}
\end{aligned} \tag{35}$$

Inward iterations: $i : n \to 1$

$$\begin{aligned}
\hat{f}_i &= R_{i+1}\ \hat{f}_{i+1} + f_i \\
\hat{n}_i &= n_i + R_{i+1}\ \hat{n}_{i+1} + p_{C_i} \times f_i + p_{i+1} \times R_{i+1}\ \hat{f}_{i+1} \\
\tau_i &= \hat{n}_i^{\mathsf{T}}\ \hat{z}_i
\end{aligned} \tag{36}$$

Example 2.1. Consider the robot manipulator presented in Figure (2). Also, consider that all masses exist in a single point at the end of each link. This masses are m_1 and m_2. First it is necessary to obtain the quantities that will appear in the Newton-Euler Algorithm. The center of mass of each link is

$$\begin{aligned}
p_{C_1} &= \ell_1, \\
p_{C_2} &= \ell_2.
\end{aligned} \tag{37}$$

Assuming the punctual mass concept, the inertia tensor of each link is a zero matrix

$$\begin{aligned} J_{C_1} &= 0, \\ J_{C_2} &= 0. \end{aligned} \tag{38}$$

This assumption leads to

$$\begin{aligned} n_1 &= \begin{bmatrix} 0 & 0 & 0 \end{bmatrix}^\intercal, \\ n_2 &= \begin{bmatrix} 0 & 0 & 0 \end{bmatrix}^\intercal. \end{aligned} \tag{39}$$

Since the robot base is not moving, we obtain

$$\begin{aligned} \omega_0 &= 0, \\ \dot{\omega}_0 &= 0, \\ \dot{v}_0 &= 0. \end{aligned} \tag{40}$$

The rotation about successive reference systems is given by

$$\begin{aligned} \text{Outward Iteration: } R_{i+1} &= \begin{bmatrix} \cos(\theta_{i+1}) & \sin(\theta_{i+1}) & 0 \\ -\sin(\theta_{i+1}) & \cos(\theta_{i+1}) & 0 \\ 0 & 0 & 1 \end{bmatrix} \\ \text{Inward Iteration: } R_{i+1} &= \begin{bmatrix} \cos(\theta_{i+1}) & -\sin(\theta_{i+1}) & 0 \\ \sin(\theta_{i+1}) & \cos(\theta_{i+1}) & 0 \\ 0 & 0 & 1 \end{bmatrix}. \end{aligned} \tag{41}$$

The Outwards iteration for link 1 can be written as follows:

$$\begin{aligned} \omega_1 &= \dot{\theta}_1 \hat{z}_1 = \begin{bmatrix} 0 \\ 0 \\ \dot{\theta}_1 \end{bmatrix}, \\ \dot{\omega}_1 &= \ddot{\theta}_1 \hat{z}_1 = \begin{bmatrix} 0 \\ 0 \\ \ddot{\theta}_1 \end{bmatrix}, \\ \dot{v}_1 &= \begin{bmatrix} \cos(\theta_1) & \sin(\theta_1) & 0 \\ -\sin(\theta_1) & \cos(\theta_1) & 0 \\ 0 & 0 & 1 \end{bmatrix} \begin{bmatrix} 0 \\ 0 \\ 0 \end{bmatrix} = \begin{bmatrix} 0 \\ 0 \\ 0 \end{bmatrix}, \\ \dot{v}_{C_1} &= \begin{bmatrix} 0 \\ 0 \\ \ddot{\theta}_1 \end{bmatrix} \times \begin{bmatrix} \ell_1 \\ 0 \\ 0 \end{bmatrix} + \begin{bmatrix} 0 \\ 0 \\ \dot{\theta}_1 \end{bmatrix} \left(\begin{bmatrix} 0 \\ 0 \\ \dot{\theta}_1 \end{bmatrix} \times \begin{bmatrix} \ell_1 \\ 0 \\ 0 \end{bmatrix} \right) = \begin{bmatrix} 0 \\ \ell_1 \ddot{\theta}_1 \\ 0 \end{bmatrix} + \begin{bmatrix} -\ell_1 \dot{\theta}_1^2 \\ 0 \\ 0 \end{bmatrix} = \begin{bmatrix} -\ell_1 \dot{\theta}_1^2 \\ \ell_1 \ddot{\theta}_1 \\ 0 \end{bmatrix}, \\ f_1 &= \begin{bmatrix} -m_1 \ell_1 \dot{\theta}_1^2 \\ m_1 \ell_1 \ddot{\theta}_1 \\ 0 \end{bmatrix}. \end{aligned} \tag{42}$$

The Outwards iteration for link 2 can be written in the form of:

$$\omega_2 = \begin{bmatrix} \cos(\theta_1) & \sin(\theta_1) & 0 \\ -\sin(\theta_1) & \cos(\theta_1) & 0 \\ 0 & 0 & 1 \end{bmatrix} \begin{bmatrix} 0 \\ 0 \\ \dot{\theta}_1 \end{bmatrix} + \begin{bmatrix} 0 \\ 0 \\ \dot{\theta}_2 \end{bmatrix} = \begin{bmatrix} 0 \\ 0 \\ \dot{\theta}_1 + \dot{\theta}_2 \end{bmatrix},$$

$$\dot{\omega}_2 = \begin{bmatrix} \cos(\theta_1) & \sin(\theta_1) & 0 \\ -\sin(\theta_1) & \cos(\theta_1) & 0 \\ 0 & 0 & 1 \end{bmatrix} \begin{bmatrix} 0 \\ 0 \\ \ddot{\theta}_1 \end{bmatrix} + \begin{bmatrix} 0 \\ 0 \\ \ddot{\theta}_2 \end{bmatrix} = \begin{bmatrix} 0 \\ 0 \\ \ddot{\theta}_1 + \ddot{\theta}_2 \end{bmatrix},$$

$$\dot{v}_2 = \begin{bmatrix} \cos(\theta_2) & \sin(\theta_2) & 0 \\ -\sin(\theta_2) & \cos(\theta_2) & 0 \\ 0 & 0 & 1 \end{bmatrix} \begin{bmatrix} -\ell_1\dot{\theta}_1^2 \\ \ell_1\ddot{\theta}_1 \\ 0 \end{bmatrix} = \begin{bmatrix} \ell_1\ddot{\theta}_1\sin(\theta_2) - \ell_1\dot{\theta}_1^2\cos(\theta_2) \\ \ell_1\ddot{\theta}_1\cos(\theta_2) + \ell_1\dot{\theta}_1^2\sin(\theta_2) \\ 0 \end{bmatrix}, \tag{43}$$

$$\dot{v}_{C_2} = \begin{bmatrix} 0 \\ \ell_2(\ddot{\theta}_1 + \ddot{\theta}_2) \\ 0 \end{bmatrix} + \begin{bmatrix} -\ell_2(\dot{\theta}_1 + \dot{\theta}_2)^2 \\ 0 \\ 0 \end{bmatrix} + \begin{bmatrix} \ell_1\ddot{\theta}_1\sin(\theta_2) - \ell_1\dot{\theta}_1^2\cos(\theta_2) \\ \ell_1\ddot{\theta}_1\cos(\theta_2) + \ell_1\dot{\theta}_1^2\sin(\theta_2) \\ 0 \end{bmatrix},$$

$$f_2 = \begin{bmatrix} m_2\ell_1\ddot{\theta}_1\sin(\theta_2) - m_2\ell_1\dot{\theta}_1^2\cos(\theta_2) - m_2\ell_2(\dot{\theta}_1 + \dot{\theta}_2)^2 \\ m_2\ell_1\ddot{\theta}_1\cos(\theta_2) + m_2\ell_1\dot{\theta}_1^2\sin(\theta_2) + m_2\ell_2(\ddot{\theta}_1 + \ddot{\theta}_2) \\ 0 \end{bmatrix}.$$

The Inwards iteration for link 2 can be written as above:

$$\hat{f}_2 = f_2,$$

$$\hat{n}_2 = \begin{bmatrix} 0 \\ 0 \\ m_2\ell_1\ell_2\cos(\theta_2)\ddot{\theta}_1 + m_2\ell_1\ell_2\sin(\theta_2)\dot{\theta}_1^2 + m_2\ell_2^2(\ddot{\theta}_1 + \ddot{\theta}_2) \end{bmatrix}. \tag{44}$$

The Inwards iteration for link 1 can be written as follows:

$$\hat{f}_1 = \begin{bmatrix} \cos(\theta_2) & -\sin(\theta_2) & 0 \\ \sin(\theta_2) & \cos(\theta_2) & 0 \\ 0 & 0 & 1 \end{bmatrix} \begin{bmatrix} m_2\ell_1\ddot{\theta}_1 \sin(\theta_2) - m_2\ell_1\dot{\theta}_1^2 \cos(\theta_2) - m_2\ell_2(\dot{\theta}_1 + \dot{\theta}_2)^2 \\ m_2\ell_1\ddot{\theta}_1 \cos(\theta_2) + m_2\ell_1\dot{\theta}_1^2 \sin(\theta_2) + m_2\ell_2(\ddot{\theta}_1 + \ddot{\theta}_2) \\ 0 \end{bmatrix} + \begin{bmatrix} -m_1\ell_1\dot{\theta}_1^2 \\ m_1\ell_1\ddot{\theta}_1 \\ 0 \end{bmatrix},$$

$$\hat{n}_1 = \begin{bmatrix} 0 \\ 0 \\ m_2\ell_1\ell_2 \cos(\theta_2)\ddot{\theta}_1 + m_2\ell_1\ell_2 \sin(\theta_2)\dot{\theta}_1^2 + m_2\ell_2^2(\ddot{\theta}_1 + \ddot{\theta}_2) \end{bmatrix} + \begin{bmatrix} 0 \\ 0 \\ m_1\ell_1^2\ddot{\theta}_1 \end{bmatrix} + \begin{bmatrix} 0 \\ 0 \\ m_2\ell_1^2\ddot{\theta}_1 - m_2\ell_1\ell_2 \sin(\theta_2)(\dot{\theta}_1 + \dot{\theta}_2)^2 + m_2\ell_1\ell_2 \cos(\theta_2)(\ddot{\theta}_1 + \ddot{\theta}_2) \end{bmatrix} \tag{45}$$

Finally, the torques can be found by extracting the $\hat{z}$ components of $\hat{n}$ i.e $\hat{n}^{\mathsf{T}}[0\,0\,1]^{\mathsf{T}}$, leading to the following torques

$$\begin{aligned} &m_2\ell_2^2(\ddot{\theta}_1 + \ddot{\theta}_2) + m_2\ell_1\ell_2 \cos(\theta_2)(2\ddot{\theta}_1 + \ddot{\theta}_2) + (m_1 + m_2)\ell_1^2\ddot{\theta}_1 - \\ &m_2\ell_1\ell_2 \sin(\theta_2)\dot{\theta}_2^2 - 2m_2\ell_1\ell_2 \sin(\theta_2)\dot{\theta}_1\dot{\theta}_2 = \tau_1, \\ &m_2\ell_1\ell_2 \cos(\theta_2)\ddot{\theta}_1 + m_2\ell_1\ell_2 \sin(\theta_2)\dot{\theta}_1^2 + m_2\ell_2^2(\ddot{\theta}_1 + \ddot{\theta}_2) = \tau_2. \end{aligned} \tag{46}$$

2.6 Quaternions

In three dimensions, a rotation can be defined by the three Euler angles i.e. (θ, β, γ). Assuming that the first rotation is performed in the z axis (θ angle), the second at the y axis (β angle), and the last at the x axis (γ angle). The matrix that allows us to determine the resultant column vector, in Cartesian coordinates, is written as the product of the three individual matrices. Each matrix represent one of the rotations presented below

$$D(\theta, \beta, \gamma) = D_1(\gamma)D_2(\beta)D_3(\theta), \text{ where:}$$

$$D_1(\gamma) = \begin{pmatrix} \cos(\gamma) & \sin(\gamma) & 0 \\ -\sin(\gamma) & \cos(\gamma) & 0 \\ 0 & 0 & 1 \end{pmatrix}; D_2(\beta) = \begin{pmatrix} 1 & 0 & 0 \\ 0 & \cos(\beta) & \sin(\beta) \\ 0 & -\sin(\beta) & \cos(\beta) \end{pmatrix}; D_3(\theta) = \begin{pmatrix} \cos(\theta) & \sin(\theta) & 0 \\ -\sin(\theta) & \cos(\theta) & 0 \\ 0 & 0 & 1 \end{pmatrix}.$$

The result is the rotation matrix presented below that is dependent on trigonometrical nonlinearities

$$D_{(\theta,\beta,\gamma)} = \begin{bmatrix} \cos(\theta)\cos(\gamma) - \sin(\theta)\cos(\beta)\sin(\gamma) & \sin(\theta)\cos(\gamma) + \cos(\theta)\cos(\beta)\sin(\gamma) & \sin(\beta)\sin(\gamma) \\ -\cos(\theta)\sin(\gamma) - \sin(\theta)\cos(\beta)\cos(\gamma) & -\sin(\theta)\sin(\gamma) + \cos(\theta)\cos(\beta)\cos(\gamma) & \sin(\beta)\cos(\gamma) \\ \sin(\beta)\sin(\gamma) & -\cos(\theta)\sin(\beta) & \cos(\beta) \end{bmatrix}.$$

In spite of the easiness of visualization and development of the Euler angles representation, the trigonometrical nonlinearities are an issue when representing the system in the DAR format. For this reason, it is not an effective method for the methodology proposed in this Dissertation. To circumvent this issue the quaternions concept is introduced as follows.

The definition of quaternion was first devised by HAMILTON (1848) as hyper-complex numbers that belong to the space $\mathbb{H}$, usually described as $q = \eta + \epsilon_1 i + \epsilon_2 j + \epsilon_3 k$ (DIEBEL, 2006).

According to Euler's rotational theorem, the relative orientation of two tridimensional coordinate systems can always be described with a single rotation angle $\psi \in \mathbb{R}$ about an unit vector $r \in \mathbb{R}^3$ depicted in Figure (3). Most times it is useful to work with quaternions in a simple linear algebra framework, combining the real part η and the imaginary part ϵ in a single $\mathbb{R}^4$ vector, as follows (DIEBEL, 2006)

$$q = \begin{bmatrix} \eta \\ \epsilon \end{bmatrix} = \begin{bmatrix} \cos(\frac{\psi}{2}) \\ r\sin(\frac{\psi}{2}) \end{bmatrix}, \tag{47}$$

where $\eta \in \mathbb{R}$ and $\epsilon \in \mathbb{R}^3$. A rotation quaternion is also by definition a unit vector, i.e.

$$\|q\| = \sqrt{\eta^2 + \epsilon^{\mathsf{T}}\epsilon} = 1\ . \tag{48}$$

Consider two quaternions q_a and q_b, the quaternion operations are defined as (KUIPERS et al., 1999):

$$Product : q_a \otimes q_b = Q(q_a)q_b \tag{49a}$$

$$\text{where } Q = \begin{bmatrix} \eta & -\epsilon^{\mathsf{T}} \\ \epsilon & \eta I + S(\epsilon) \end{bmatrix} \tag{49b}$$

$$Conjugate : q^* = \begin{bmatrix} \eta \\ -\epsilon \end{bmatrix} \tag{49c}$$

$$Norm : ||q|| = \sqrt{\eta^2 + \epsilon^{\mathsf{T}}\epsilon} \tag{49d}$$

$$Inverse : q^{-1} = \frac{q^*}{||q||}. \tag{49e}$$

Figure 3 – Quaternion axis-angle representation.

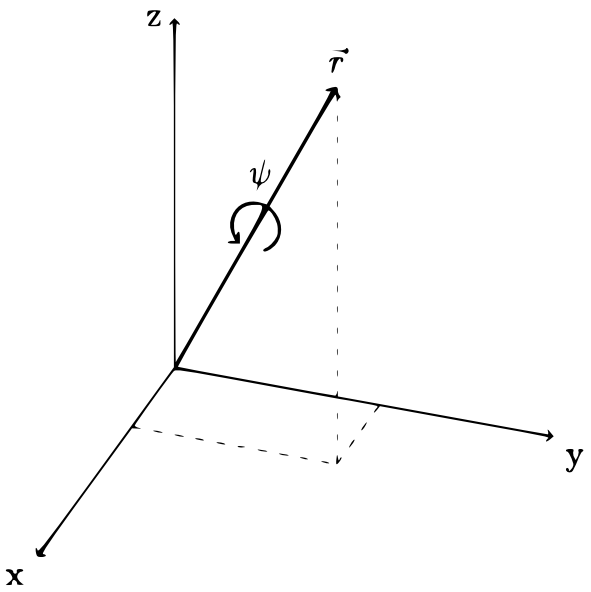

Source: SALTON et al. (2017).

It can be shown that the desired rotation can be applied to an ordinary vector $p = (p_x, p_y, p_z)$ in a three-dimensional space, considering p as a quaternion with a real component equal to zero, by evaluating the conjugation of p by q

$$p' = q \otimes p \otimes q^{-1}$$

using the quaternion product, where p' is the new position vector after the rotation.

A rotation quaternion $p' = q \otimes p \otimes q^{-1}$ can be algebraically manipulated into a matrix rotation $p' = R(q)p$, where $R(q)$ is the matrix rotation given by

$$R(q) = \begin{bmatrix} 1 - 2(\epsilon_2^2 + \epsilon_3^2) & 2(\epsilon_1\epsilon_2 - \epsilon_3\eta) & 2(\epsilon_1\epsilon_3 - \epsilon_2\eta) \\ 2(\epsilon_1\epsilon_2 + \epsilon_3\eta) & 1 - 2(\epsilon_1^2 + \epsilon_3^2) & 2(\epsilon_2\epsilon_3 - \epsilon_1\eta) \\ 2(\epsilon_1\epsilon_3 - \epsilon_2\eta) & 2(\epsilon_2\epsilon_3 + \epsilon_1\eta) & 1 - 2(\epsilon_1^2 + \epsilon_2^2) \end{bmatrix}$$

$$R(q) = I_3 + 2\eta S(\epsilon) + 2S(\epsilon)^2, R(q) \in \mathbb{R}^3 \tag{50}$$

where I_3 is the identity matrix , and $S(\cdot)$ denotes

$$S(z) = \begin{bmatrix} 0 & -z_3 & z_2 \\ z_3 & 0 & -z_1 \\ -z_2 & z_1 & 0 \end{bmatrix},$$

which is used to represent a vector cross product in matrix form, i.e. $a \times b = S(a)b$.

The application of calculus theory in the set of quaternion numbers has led to a dynamic description of continuously rotating frames. Suppose a local frame is rotating with angular velocity $\omega \in \mathbb{R}^3$. Then, the rate of change of the local frame orientation is given by:

$$\dot{q} = G(q)\omega \tag{51}$$

where the transformation matrix $G(q)$ is

$$G(q) = \frac{1}{2}\begin{bmatrix} -\epsilon^{\mathsf{T}} \\ \eta I + S(\epsilon) \end{bmatrix} \tag{52}$$

2.7 Final Remarks

This chapter introduced the concept of stability for nonlinear systems. A quick review of the algebraic differential representation is presented along with a collection of LMI based Lemmas, including the stability of nonlinear systems with control input saturation. The chapter then brought the Newton-Euler Algorithm used to construct an n-link manipulator model illustrated by a 2-link manipulator example. Quaternion concepts and properties that will be part of the dissertation methodology were also presented.

3 Two Link Manipulator Model

N-link manipulators are known for the high complexity of their model. This complexity comes from the fact that each link of a manipulator can be seen as a rigid solid body influencing the motion of other links. This chain of motion appears in the model as high order trigonometric nonlinearities. So the contribution of this chapter lies in a representation of the system such that the control design may later be cast as a convex optimization problem subject to LMIs. It is important to state that no linearization or any other kind of approximation is employed in the presented method, which consists in describing the system in a Differential-Algebraic Representation, as presented in Chapter 2.

To illustrate the method, consider the following model from example 2.1, where rotations are represented by the Euler angles. By reorganizing the terms in equation (46), the following system is presented:

$$\begin{aligned} \omega &= \dot{\theta} \\ M(\theta)\dot{\omega} + v(\theta,\omega) &= u \end{aligned} \tag{53}$$

$$M(\theta) = \begin{bmatrix} \ell_2^2 m_2 + 2\ell_1\ell_2 m_2\cos(\theta_2) + \ell_1^2(m_1+m_2) & \ell_2^2 m_2 + \ell_1\ell_2 m_2\cos(\theta_2) \\ \ell_2^2 m_2 + \ell_1\ell_2 m_2\cos(\theta_2) & \ell_2^2 m_2 \end{bmatrix} \tag{54}$$

$$v(\theta,\omega) = \begin{bmatrix} -m_2\ell_1\ell_2\sin(\theta_2)\omega_2^2 - 2m_2\ell_1\ell_2\sin(\theta_2)\omega_1\omega_2 \\ m_2\ell_1\ell_2\sin(\theta_2)\omega_1^2 \end{bmatrix} \tag{55}$$

In order to develop a systematic approach able to deal with the aforementioned system nonlinearities, we consider using a quaternion-based representation of the manipulator orientation. In the particular system being addressed in this Dissertation, all rotation vectors are fixed around the axis $r = [0\ 0\ 1]^\top$, for this reason, $\psi = \theta$. To represent the system presented above in quaternion bases, it is possible to substitute the rotation matrix in the Newton-Euler Algorithm by a quaternion rotation matrix or substitute the sines and cosines presented in the model by the equivalent in quaternions. When utilizing the second statement, a relation between the trigonometric functions and the quaternion must be established. It is important to notice that the use of quaternions in the modeling will allow the system model expansion to a non-planar manipulator system in future works.

Since the system (53) has only rotations around the $\hat{z}$-axis, it is possible to simplify the

quaternion as

$$q_i = \begin{bmatrix} \eta_i \\ \epsilon_i \end{bmatrix} = \begin{bmatrix} \cos\left(\frac{\theta_i}{2}\right) \\ \sin\left(\frac{\theta_i}{2}\right) \end{bmatrix}. \tag{56}$$

This simplified quaternion has only two components, the real part η and the imaginary part ϵ, where i is the link that the rotation is being performed.

As presented in chapter 2 the rotation matrix around the z-axis is given by

$$R(\theta) = \begin{bmatrix} \cos(\theta) & \sin(\theta) & 0 \\ -\sin(\theta) & \cos(\theta) & 0 \\ 0 & 0 & 1 \end{bmatrix}. \tag{57}$$

By applying the quaternion (56) into the rotation matrix (50), the following rotation matrix about the z-axis in quaternion base is obtained

$$R(q) = \begin{bmatrix} 1-2\epsilon^2 & 2\eta\epsilon & 0 \\ -2\eta\epsilon & 1-2\epsilon^2 & 0 \\ 0 & 0 & 1 \end{bmatrix}. \tag{58}$$

Then a relation can be established by

$$R(\theta) = R(q)$$

leading to:

$$\begin{aligned} \cos(\theta_i) &= 1 - 2\epsilon_i^2 \\ \sin(\theta_i) &= 2\eta_i\epsilon_i. \end{aligned} \tag{59}$$

Now, through the (51), it is possible to represent system (53) entirely in quaternion base. The quaternion system is given by

$$\begin{aligned} \dot{\eta} &= -\frac{1}{2}\epsilon\omega \\ \dot{\epsilon} &= \frac{1}{2}\eta\omega \\ M(q)\dot{\omega} &= u - v(q,\omega) \end{aligned} \tag{60}$$

where

$$M(q) = \begin{bmatrix} \ell_2^2 m_2 + 2\ell_1\ell_2 m_2(1-2\epsilon_2^2) + \ell_1^2(m_1+m_2) & \ell_2^2 m_2 + \ell_1\ell_2 m_2(1-2\epsilon_2^2) \\ \ell_2^2 m_2 + \ell_1\ell_2 m_2(1-2\epsilon_2^2) & \ell_2^2 m_2 \end{bmatrix} \tag{61}$$

$$v(q,\omega) = \begin{bmatrix} -m_2\ell_1\ell_2(2\eta_2\epsilon_2)\omega_2^2 - 2m_2\ell_1\ell_2(2\eta_2\epsilon_2)\omega_1\omega_2 \\ m_2\ell_1\ell_2(2\eta_2\epsilon_2)\omega_1^2 \end{bmatrix} \tag{62}$$

In order to represent the difference between the desired reference attitude q_{r_i} (associated to reference angles θ_{r_i}) and the actual manipulator attitude q_i, we consider using an error quaternion defined by the following relation:

$$q_{e_i} = q_{r_i}^{-1} \otimes q_i = \begin{bmatrix} \eta_{e_i} \\ \epsilon_{e_i} \end{bmatrix} = \begin{bmatrix} \eta_{r_i}\eta_i + \epsilon_{r_i}^{\mathsf{T}}\epsilon_i \\ \eta_{r_i}\epsilon_i - \epsilon_{r_i}\eta_i \end{bmatrix} . \tag{63}$$

From the fundamentals of the quaternion algebra (KUIPERS et al., 1999), it follows that if both q_{r_i} and q_i are unit quaternions, then the result q_{e_i} from relation is also a unit quaternion. Furthermore, one should verify that, when q_i approaches its reference q_{r_i}, the error quaternion q_{e_i} approaches the unity, i.e.

$$q_i \to \pm q_{r_i} \;\; \Rightarrow \;\; \eta_{e_i} \to \pm 1 \; , \; \epsilon_{e_i} \to 0 \; . \tag{64}$$

recalling that for every unit quaternion q, its opposite $-q$ represents an identical rotation. From the unit norm property highlighted in (48), $\epsilon_{e_i} \to 0$ readily implies that $\eta_{e_i} \to \pm 1$, therefore one gets that

$$\epsilon_{e_i} \to 0 \;\Leftrightarrow\; \theta_i \to \theta_{r_i} \; . \tag{65}$$

The robotic manipulator attitude tracking problem is consequently equivalent to the asymptotic stabilization of ϵ_{e_i} with respect to zero.

As a dynamic reference can be considered in (63), the model complexity could increase significantly. So, to maintain the model simplicity, a constant reference q_{r_i} is considered. By taking the time derivative of (63), the error dynamics can be described by the following equation

$$\begin{aligned} \dot{\eta}_{e_i} &= -\frac{1}{2}\epsilon_{e_i}\omega_i \\ \dot{\epsilon}_{e_i} &= \frac{1}{2}\eta_{e_i}\omega_i. \end{aligned} \tag{66}$$

Noticeably from (65), it suffices to work only with the dynamics of ϵ_{e_i} and the parameter η_{e_i} may be regarded as a function of ϵ_{e_i} according to the unit norm constraint:

$$\eta_{e_i} = \pm\sqrt{1 - \epsilon_{e_i}^2} \; . \tag{67}$$

In order to deal with duality in the sign of the above relation, we introduce a quaternion coordinate transformation similarly as presented in (SALTON et al., 2017).

This is equivalent to ensure the restriction of the link error angles within $(-\pi, \pi)$, in which case, we can finally express that

$$\dot{\varepsilon}_{e_i} = \frac{1}{2}|\eta_{e_i}|\,\omega_i \; . \tag{68}$$

Therefore, η_{e_i} will be dropped from the equations and, considering (66), the system can be described as:

$$\begin{aligned} \dot{\varepsilon}_e =& \frac{1}{2}\begin{bmatrix} |\eta_{e_1}| & 0 \\ 0 & |\eta_{e_2}| \end{bmatrix}\omega \\ M(q)\dot{\omega} =& u - \mathrm{v}(q,\omega). \end{aligned} \tag{69}$$

In order to simplify the construction of the robotic manipulator DAR, the equations of motion related to the angular velocities ω are being deliberately expressed in terms of the absolute quaternions q.

$$M(q) = \begin{bmatrix} \ell_2^2 m_2 + 2\ell_1\ell_2 m_2(1-2\epsilon_2^2) + \ell_1^2(m_1+m_2) & \ell_2^2 m_2 + \ell_1\ell_2 m_2(1-2\epsilon_2^2) \\ \ell_2^2 m_2 + \ell_1\ell_2 m_2(1-2\epsilon_2^2) & \ell_2^2 m_2 \end{bmatrix}, \tag{70}$$

$$\mathrm{v}(q,\omega) = \begin{bmatrix} -2m_2\ell_1\ell_2\eta_2\epsilon_2(2\omega_1\omega_2 + \omega_2^2) \\ 2m_2\ell_1\ell_2\eta_2\epsilon_2\omega_1^2 \end{bmatrix}. \tag{71}$$

Notice that to represent system (69) in the (24) format it would be necessary to multiply both sides of (53) by the inverse of the inertia matrix $M(q,\omega)$, so as to isolate the angular acceleration vector component $\dot{\omega}$, a procedure that would significantly increase the complexity of the system dynamics. To avoid this difficulty, we propose in this Dissertation a new DAR structure with descriptor components, which will allow to directly address (53) without the complete inversion of $M(q,\omega)$. For instance, our DAR is expanded as

$$\begin{cases} A_0\dot{x} &= A_1(x,\delta)x + A_2(x,\delta)\xi + A_3(\delta)\dot{x} + Bu \\ 0 &= \Omega_1(x,\delta)x + \Omega_2(x,\delta)\xi + \Omega_3(x,\delta)u \end{cases} \tag{72}$$

where $A_0 \in \mathbb{R}^4$ contains the constant terms that are multiplying $\dot{x}$ and $A_3(\delta) \in \mathbb{R}^4$ contains the nonlinear terms that are multiplying $\dot{x}$.

To represent system (69) in (72) format, consider the state variables given by

$$x = \begin{bmatrix} \varepsilon_{e_1} & \varepsilon_{e_2} & \omega_1 & \omega_2 \end{bmatrix}^{\mathsf{T}}, \tag{73}$$

which contains the angular velocities ω_i and the ε_{e_i} components of the error quaternions q_{e_i}. In turn, the domain of interest related to these variables is specified as

$$\mathcal{X} = \Big\{ x \in \mathbb{R}^4 : |x_i| \leq \sin(\overline{\theta}_{e_i}/2),\ |x_{i+2}| \leq \overline{\omega}_i,\ i = 1,2 \Big\}, \tag{74}$$

where $0 < \overline{\theta}_{e_i} < \pi$ and $\overline{\omega}_i > 0$ are denoting the maximum admissible angular position error and velocity of the i-th manipulator link.

Due to the complexity of some nonlinearities present in the system (69), a vector of time-varying parameters will be established in order to keep the simplicity of the method. This vector is given by

$$\delta = \begin{bmatrix} |\eta_{e_1}| & |\eta_{e_2}| & 2\eta_2\varepsilon_2 & 1 - 2\varepsilon_2^2 \end{bmatrix}. \tag{75}$$

Provided that $x \in \mathcal{X}$, it directly follows that this vector δ is bounded inside the following set:

$$\Delta = \Big\{ \delta \in \mathbb{R}^4 : \cos(\overline{\theta}_{e_i}/2) \leq \delta_i \leq 1,\ |\delta_{i+2}| \leq 1,\ i = 1,2 \Big\}. \tag{76}$$

It is important to notice that these uncertainties are clearly bounded due to the relation (59). By choosing these uncertainties, it is possible to write the auxiliary vector ξ as a function of the states x and the uncertainties δ represented above

$$\xi = \begin{bmatrix} \delta_3 x_4 & \delta_3 x_3 \end{bmatrix}^\intercal . \tag{77}$$

Given these definitions for x, δ and ξ, the robotic manipulator system introduced in the previous section can be expressed in the descriptor DAR (72) with the following matrices:

$$\begin{aligned}
A_0 &= \begin{bmatrix} 1 & 0 & 0 & 0 \\ 0 & 1 & 0 & 0 \\ 0 & 0 & (m_1+m_2)\ell_1^2 + m_2\ell_2^2 & \ell_2^2 m_2 \\ 0 & 0 & \ell_2^2 m_2 & \ell_2^2 m_2 \end{bmatrix} \\
A_1(\delta) &= \frac{1}{2}\begin{bmatrix} 0 & 0 & \delta_1 & 0 \\ 0 & 0 & 0 & \delta_2 \\ 0 & 0 & 0 & 0 \\ 0 & 0 & 0 & 0 \end{bmatrix} \\
A_2(x) &= \begin{bmatrix} 0 & 0 \\ 0 & 0 \\ m_2\ell_1\ell_2 x_4 + 2m_2\ell_1\ell_2 x_3 & 0 \\ 0 & -m_2\ell_1\ell_2 x_3 \end{bmatrix} \\
A_3(\delta) &= \begin{bmatrix} 0 & 0 & 0 & 0 \\ 0 & 0 & 0 & 0 \\ 0 & 0 & -2m_2\ell_1\ell_2\delta_4 & -m_2\ell_1\ell_2\delta_4 \\ 0 & 0 & -m_2\ell_1\ell_2\delta_4 & 0 \end{bmatrix} \quad B = \begin{bmatrix} 0 & 0 \\ 0 & 0 \\ 1 & 0 \\ 0 & 1 \end{bmatrix} \\
\Omega_1(\delta) &= \begin{bmatrix} 0 & 0 & 0 & \delta_3 \\ 0 & 0 & \delta_3 & 0 \end{bmatrix} \quad \Omega_2 = \begin{bmatrix} -1 & 0 \\ 0 & -1 \end{bmatrix}
\end{aligned} \tag{78}$$

By now using an augmented vector $\xi_a = [\xi^\intercal \;\; \dot{x}^\intercal]^\intercal \in \mathbb{R}^6$ that combines ξ with $\dot{x}$, we can show that the descriptor DAR from (72) can be re-arranged to appear as a traditional DAR, such as the one in (24). In this case, we simply need to include an extra equality constraint related to state derivatives, i.e.,

$$0 = A_1(\delta)\, x + A_2(x)\, \xi + (A_3(\delta) - A_0)\, \dot{x} + B\, u. \tag{79}$$

Moreover, since all of the descriptor nonlinearities were grouped into $A_3(\delta)\,\dot{x}$, the invariant descriptor component $A_0\,\dot{x}$ can be cancelled out by inversion of A_0, which is clearly non-singular from (78). This process allows one to re-write (72) as

$$\begin{cases} \dot{x} = \mathbf{A_1}(\delta)x + \mathbf{A_2}(x,\delta)\xi_a + \mathbf{B}u \\ 0 = \mathbf{\Omega_1}(\delta)x + \mathbf{\Omega_2}(x,\delta)\xi_a + \mathbf{\Omega_3}u \end{cases}, \tag{80}$$

where the augmented matrices shown in here are constructed in the following manner:

$$\mathbf{A_1}(\delta) = A_0^{-1}A_1(\delta)\,,\;\; \mathbf{A_2}(x,\delta) = A_0^{-1}\begin{bmatrix} A_2(x) & A_3(\delta)\end{bmatrix},$$

$$\mathbf{\Omega}_1(\delta) = \begin{bmatrix}\Omega_1(\delta)\\ A_1(\delta)\end{bmatrix},\;\; \mathbf{\Omega}_2(x,\delta) = \begin{bmatrix}\Omega_2 & 0\\ A_2(x) & A_3(\delta)-A_0\end{bmatrix}, \tag{81}$$

$$\mathbf{B} = A_0^{-1}B\,,\;\; \mathbf{\Omega}_3 = \begin{bmatrix}0\\ B\end{bmatrix}.$$

It is important to notice that matrix $\mathbf{\Omega}_2$ must be non-singular i.e. $det(\mathbf{\Omega}_2) \neq 0\,\forall\, x,\, \delta$ knowing that for any real mechanical system the inertia matrix $M = A_0 - A_3$ will always be non-singular, so by assuring an Ω_2 that is non-singular the condition for $\mathbf{\Omega}_2$ is fulfilled. This representation will subsequently allow us to cast the manipulator control design problem in terms of a semidefinite optimization problem, in which the objective is to ensure the asymptotic stability of the system trajectories and considering all nonlinearities of the planar manipulator.

3.1 Final Remarks

This chapter brings the methodology used to convert the well-know 2-link manipulator model into the DAR representation. A quaternion-based model is presented, along with a change of coordinates in order to include the error dynamics into the system. The system states x, the vector $\delta(x)$ and the nonlinear auxiliary vector $\xi(x)$ are presented. The main contribution of the dissertation is presented by representing the DAR system via the innovative descriptor representation by constructing matrices $\mathbf{A}_1(\delta)$, $\mathbf{A}_2(x,\delta)$, $\mathbf{B}$, $\mathbf{\Omega}_1(\delta)$, $\mathbf{\Omega}_2(x,\delta)$ and $\mathbf{\Omega}_3$.

4 Control Design

A systematic methodology based on the differential-algebraic representation is proposed in this chapter, aiming to ensure the system closed-loop stability via a control design for rational nonlinear systems without any kind of linearization.

Our primary control objective is to ensure the asymptotic stabilization of the trajectories $x(t)$ of system (80) with respect to the origin for a given set of admissible initial conditions $x(0) \in \mathcal{R}$, recalling that $\|x\| \to 0$ means that the manipulator configuration approaches and settles in a prescribed reference attitude defined by the reference quaternions. In this sense, we want to systematically synthesize a control law such that a domain of attraction estimate $\mathcal{R}$ is made as large as possible.

In order to do that, the robotic manipulator control law is considered as

$$u = Kx, \tag{82}$$

where K is the feedback gain matrix. In this proposal, the following performance criterion is going to be considered besides the asymptotic stabilization.

Definition 4.1. *Exponential performance*: The system trajectories $x(t)$ exponentially approach the origin with decay rate faster than $\lambda > 0$, i.e. $\exists\, \kappa : \|x(t)\| \leq \kappa\, \mathrm{e}^{-\lambda t}\, \forall\, x(0) \in \mathcal{R}$

Prior to showing our results it is also convenient to re-express the domain of interest $\mathcal{X}$ from (74) in a standard polyhedral form such as

$$\mathcal{X} = \left\{ x \in \mathbb{R}^4 : |\alpha_k x_k| \leq 1\,, k = 1,2,3,4 \right\}, \tag{83}$$

where the vectors $\alpha_1, \alpha_2, \alpha_3, \alpha_4 \in \mathbb{R}^{1\times 4}$ are defined by

$$\begin{aligned} \alpha_1 &= [\sin(\overline{\theta}_{e_1}/2)^{-1} \;\; 0 \;\; 0 \;\; 0]\,, \quad \alpha_3 = [0 \;\; 0 \;\; \overline{\omega}_1^{-1} \;\; 0]\,, \\ \alpha_2 &= [0 \;\; \sin(\overline{\theta}_{e_2}/2)^{-1} \;\; 0 \;\; 0]\,, \quad \alpha_4 = [0 \;\; 0 \;\; 0 \;\; \overline{\omega}_2^{-1}]\,. \end{aligned} \tag{84}$$

The following theorem is proposed in order to design the controller. The theorem is adapted from (CASTRO, 2019).

Theorem 4.1. *Consider the system* (68) *and its DAR* (80) *subject to the control law* (82)*. Suppose there exist a matrix* $\hat{P} \in \mathbb{R}^{4\times 4}$ *and generic matrices* $\hat{L} \in \mathbb{R}^{4\times 4}$ *and* $\hat{K} \in \mathbb{R}^{2\times 4}$ *such that:*

$$\hat{P} > 0, \tag{85}$$

$$\begin{bmatrix} 1 & \alpha_k \hat{P} \\ \star & \hat{P} \end{bmatrix} > 0\, \forall\, k = 1,2,3,4, \tag{86}$$

$$\mathrm{He}\left\{\begin{bmatrix}\mathbf{A}_1(\delta)\hat{P}+\lambda\hat{P}+\mathbf{B}\hat{K} & \mathbf{A}_2(x,\delta)\hat{L}\\ \boldsymbol{\Omega}_1(\delta)\hat{P}+\boldsymbol{\Omega}_3\hat{K} & \boldsymbol{\Omega}_2(x,\delta)\hat{L}\end{bmatrix}\right\}<0, \tag{87}$$

$\forall(x,\delta)\in\mathcal{V}(\mathcal{X})\times\mathcal{V}(\Delta)$. *Then, all closed loop system trajectories with* $K=\hat{K}\hat{P}^{-1}$ *asymptotically approach the origin with decay rate greater then* λ *and satisfy the exponential criterion for all initial conditions* $x(0)$ *starting in the region:*

$$\mathcal{R}=\{x\in\mathbb{R}^4 : x^{\mathsf{T}}\hat{P}^{-1}x\leq 1\}. \tag{88}$$

Proof. Consider a Lyapunov candidate function as:

$$V(x)=x^{\mathsf{T}}Px, \tag{89}$$

with $P>0$ in order to ensure that $V(x)>0\,\forall\, x\neq 0$. The derivative of (89) along the trajectories of (80) is given by:

$$\dot{V}(x,\delta)=\begin{bmatrix}x^{\mathsf{T}} & \xi_a^{\mathsf{T}}\end{bmatrix}\mathrm{He}\left\{\begin{bmatrix}P(\mathbf{A}_1(\delta)+\mathbf{B}K) & P\mathbf{A}_2(x,\delta)\\ 0 & 0\end{bmatrix}\right\}\begin{bmatrix}x\\ \xi_a\end{bmatrix}. \tag{90}$$

Now, suppose the following inequality is satisfied for all $(x,\delta)\in\mathcal{X}\times\Delta$:

$$\dot{V}(x,\delta)+2\lambda V(x)+\mathrm{He}\left\{\xi_a^{\mathsf{T}}L\begin{bmatrix}\boldsymbol{\Omega}_1(\delta)+\boldsymbol{\Omega}_3K & \boldsymbol{\Omega}_2(x,\delta)\end{bmatrix}\begin{bmatrix}x\\ \xi_a\end{bmatrix}\right\}<0, \tag{91}$$

or equivalently:

$$\mathrm{He}\left\{\begin{bmatrix}P(\mathbf{A}_1(\delta)+\mathbf{B}K)+\lambda P & P\mathbf{A}_2(x,\delta)\\ L(\boldsymbol{\Omega}_1(\delta)+\boldsymbol{\Omega}_3K) & L\boldsymbol{\Omega}_2(x,\delta)\end{bmatrix}\right\}<0. \tag{92}$$

Given that $\lambda\geq 0$, $V(x)>0$ and $(\boldsymbol{\Omega}_1+\boldsymbol{\Omega}_3K)\,x+\boldsymbol{\Omega}_2\,\xi_a=0$, it follows that (91) implies that $\dot{V}(x,\delta)<0\,\forall(x,\delta)\in\mathcal{X}\times\Delta$. Pre- and post-multiplying (92) by $\mathrm{diag}\{P^{-1},L^{-T}\}$, (87) is obtained, considering the change of variables $\hat{P}=P^{-1}$ and $\hat{L}=L^{-T}$. In the same way, the relation (85) is verified when pre- and post-multiplying $P>0$ by P^{-1}.

In order to ensure that $\mathcal{R}\subset\mathcal{X}$ as required by Theorem 2.1, it is necessary and sufficient to guarantee that

$$x^{\mathsf{T}}\alpha_k^{\mathsf{T}}\alpha_k\,x<x^{\mathsf{T}}Px\leq 1\Leftrightarrow P-\alpha_k^{\mathsf{T}}\alpha_k>0\,\forall\,k=1,2,3,4. \tag{93}$$

Applying Schür's complement, this relation can be expressed as

$$\begin{bmatrix}1 & \alpha\\ \star & P\end{bmatrix}>0. \tag{94}$$

Pre- and post-multiplying (94) by $\mathrm{diag}\{1,P^{-1}\}$, (86) is obtained. Hence, according to Theorem 2.1, conditions (85), (86) and (87) guarantee that all trajectories starting in $\mathcal{R}$ asymptotically approach the origin. Beyond this fact, from the inequality presented in (91), it follows that

$$\dot{V}(x,\delta)<-2\lambda V(x), \tag{95}$$

Moreover, from relation (95), it is also noticeable that

$$V(x(t)) < V(x(0))\,\mathrm{e}^{-2\lambda t}\;\forall\, x(0) \in \mathcal{R}\,. \tag{96}$$

Since $P_{min}\|x\|^2 \leq x^{\intercal}Px = V(x)$, where P_{min} denotes the smallest eigenvalue of P, it also follows that the exponential performance criterion in Definition 4.1 holds with

$$\kappa = \sqrt{P_{min}^{-1}x^{\intercal}(0)Px(0)}. \tag{97}$$

To conclude the proof, if the LMI (87) is satisfied for (x, δ) at the cartesian product of vertices $\mathcal{V}(\mathcal{X}) \times \mathcal{V}(\Delta)$, by convexity they are also satisfied $\forall\,(x, \delta) \in \mathcal{X} \times \Delta$. □

From the domain of attraction estimate (88), it is concluded that minimizing the trace of $\hat{P}^{-1}$ implies the maximization of the sum of all semi-axes of the ellipsoidal set $\mathcal{R}$. Thus, the design of K that maximizes region $\mathcal{R}$ can be solved by the following convex optimization problem based on Theorem 4.1:

$$\begin{aligned} &\underset{N,\hat{P},\hat{L},\hat{K}}{\text{minimize}} \quad \mathrm{tr}(N) \\ &\text{subject to} \quad (85), (86), (87), \begin{bmatrix} N & I \\ \star & \hat{P} \end{bmatrix} > 0. \end{aligned} \tag{98}$$

From the application of the Schür complement in the LMI introduced in (98), where $N \in \mathbb{R}^{4\times4}$ is a symmetrical matrix and $I_4 \in \mathbb{R}^{4\times4}$ is an identity matrix, we have that $N > \hat{P}^{-1}$. Hence, recalling that $\hat{P}^{-1} = P$, minimizing the trace of N implies the maximization of the region of attraction $\mathcal{R}$, since $\mathrm{tr}(N) > \mathrm{tr}(P)$.

It is important to note that no constraint has been imposed on the gain K, this may lead to extremely high gains when synthesizing the controller by numerical optimization. In order to circumvent this issue, it is suggested to consider the following design constraint:

$$\tilde{u}_i^{-1}|K_{[i]}x| < 1\,\forall\, x \in \mathcal{R}, \tag{99}$$

where $\tilde{u}_i$ denotes the peek control value of the i-th control input signal for every trajectory inside the domain of attraction $\mathcal{R}$. Then, by noticing that (99) is equivalent to $\tilde{u}_i^{-2}x^{\intercal}K_{[i]}^{\intercal}K_{[i]}x < 1\,\forall x \in \mathcal{R}$, it follows that:

$$\begin{bmatrix} \tilde{u}_i^2 & K \\ \star & P \end{bmatrix} > 0\,\forall\, i = 1, 2, \tag{100}$$

Pre- and post-multiplying (100) by $\mathrm{diag}\{1, P^{-1}\}$, equation above is obtained

$$\begin{bmatrix} \tilde{u}_i^2 & \hat{K} \\ \star & \hat{P} \end{bmatrix} > 0\,\forall\, i = 1, 2, \tag{101}$$

Hence, one must simply include the LMI (100) into the optimization problem (98) in order restrict the peek value of each control input.

4.1 Numerical Example

This section presents a numerical simulation of a robotic manipulator control system in order to illustrate the contribution presented in this Dissertation. The numerical results were obtained in the MATLAB R2012b software and its native LMILAB toolbox was employed to solve the proposed convex optimization problem with LMI constraints. An ideal two-link manipulator is here considered with dynamics governed by equations (69), where the system parameters and the design parameters are shown in Table 1 and Table 2 respectively. Also the links references were chosen as $\theta_{r1} = 80^\circ$, $\theta_{r2} = -110^\circ$. Given these setup parameters, the proposed convex optimization problem (98) yielded the feedback matrix

$$K = \begin{bmatrix} -6969.2 & -421.2 & -3715.7 & -200.4 \\ 1811.3 & -1873.3 & 971.8 & -976.2 \end{bmatrix}, \tag{102}$$

in which case the domain of attraction estimate (88) is defined with

$$P = \begin{bmatrix} 2.2056 & 0.0000 & 0.2685 & 0.0000 \\ 0.0000 & 1.7401 & 0.0000 & 0.0192 \\ 0.2685 & 0.0000 & 0.1438 & 0.0000 \\ 0.0000 & 0.0192 & 0.0000 & 0.0102 \end{bmatrix}, \tag{103}$$

where $\mathrm{tr}(P) = 4.0997$.

Table 1 – Physical parameters of the robotic manipulator example

Parameter	Value
m_1	$10\,\mathrm{kg}$
m_2	$1\,\mathrm{kg}$
ℓ_1	$1\,\mathrm{m}$
ℓ_2	$1\,\mathrm{m}$

Figures (4) and (5) show the time series produced by a numerical simulation of the closed-loop system with the controller designed by the proposed methodology. The target reference attitude angles were defined as $\theta_{r_1} = 80^\circ$ and $\theta_{r_2} = -110^\circ$ and the initial manipulator angles as $\theta_1(0) = 103.07^\circ$ and $\theta_2(0) = -86.93^\circ$, yielding the initial errors $\theta_{e_1}(0) = \theta_{e_2}(0) = 23.07^\circ$ for both joint angles (which are equivalent to $x_1(0) = x_2(0) = 0.2$ in the quaternion error representation). In turn, the initial joint angular velocities were considered as $\omega_1(0) = x_3(0) = 2\,\mathrm{rad/s}$ and $\omega_2(0) = x_4(0) = 0\,\mathrm{rad/s}$. This system initial state is marginally close to the border of the domain of attraction estimate $\mathcal{R}$.

Table 2 – Control design parameters

Parameter	Value
$\overline{\theta}_{e_1}$	100°
$\overline{\theta}_{e_2}$	100°
$\overline{\omega}_1$	$3\,\mathrm{rad/s}$
$\overline{\omega}_2$	$10\,\mathrm{rad/s}$
λ	0.6
$\tilde{u}_1$	$10^4\,\mathrm{Nm}$
$\tilde{u}_2$	$10^4\,\mathrm{Nm}$

Figure 4 – Time series of the error angles $\theta_e(t)$ yielded by the numerical simulation.

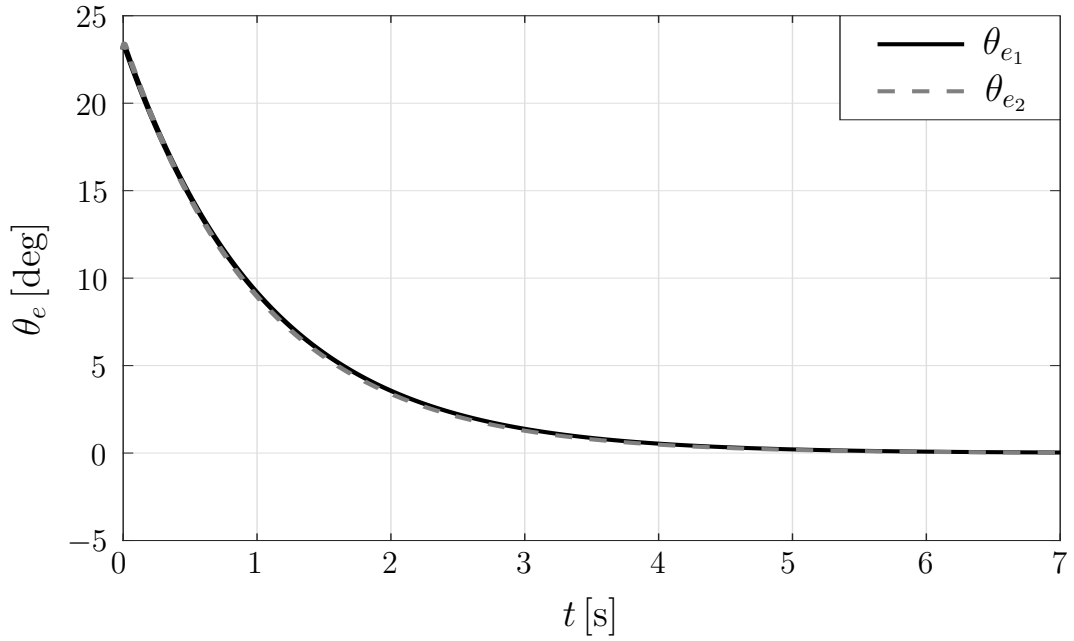

Source: the Author

Figure (6) show the time series of both links showing that the angle θ_i exponentially converges to the reference θ_{ri}. This result was also produced by a numerical simulation of the closed-loop system with the controller designed by the proposed methodology.

Figure 5 – Time series of the angular velocities $\omega(t)$ yielded by the numerical simulation.

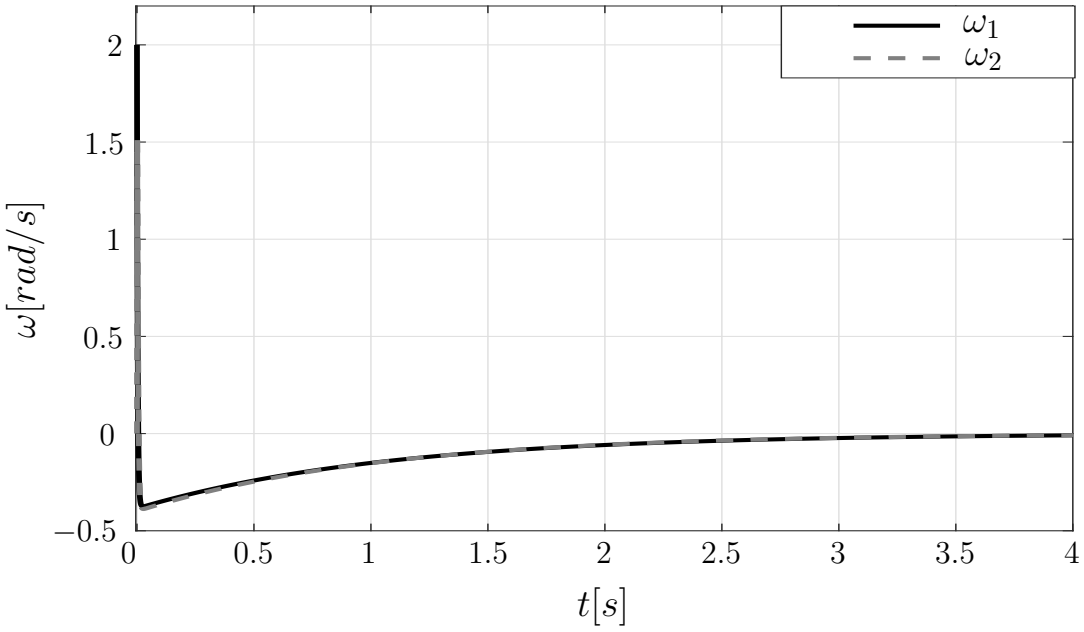

Source: the Author

Figure 6 – Time series of the link angles $\theta(t)$ yielded by the numerical simulation.

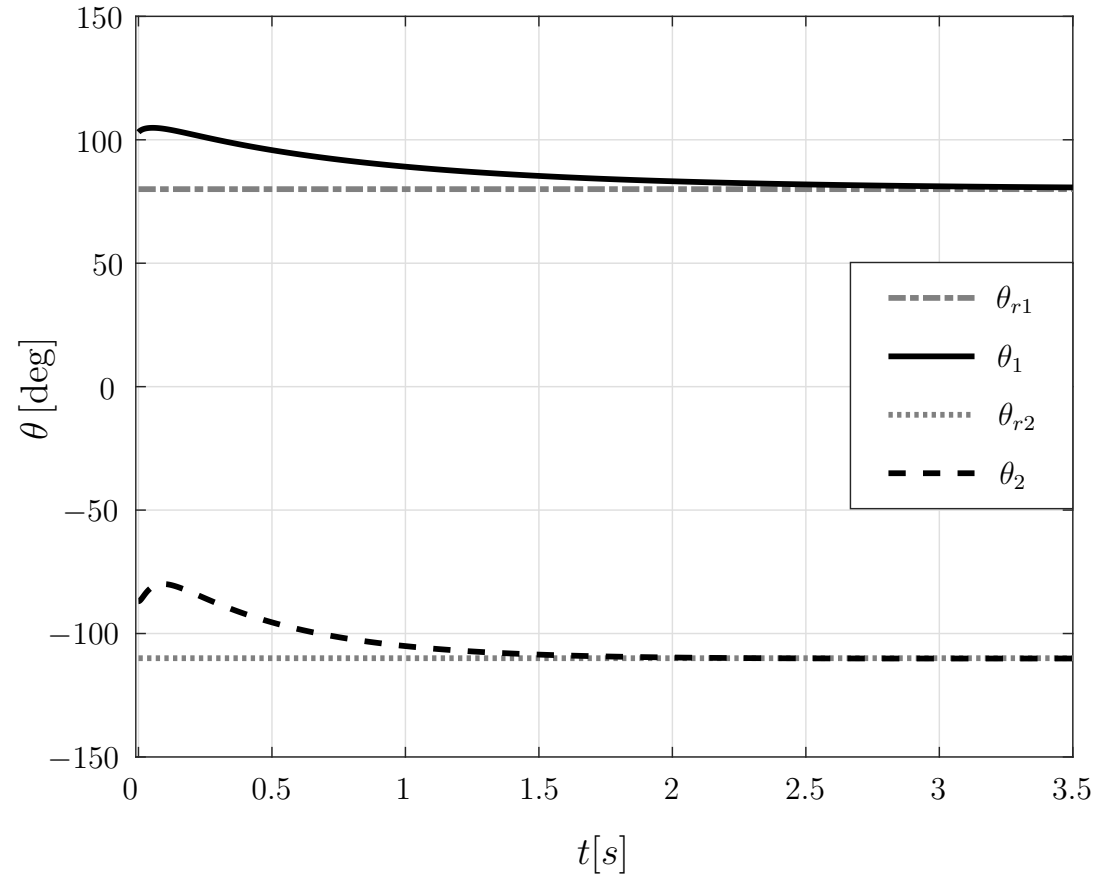

Source: the Author

Figure (7) show the time series of the control signal, it is important to notice that the maximum value of K never reach maximum admissible value of 10^4 as in Table 2, condition which is ensured by the additional constraint (100).

Figure 7 – Time series of the control signal $u(t)$ yielded by the numerical simulation.

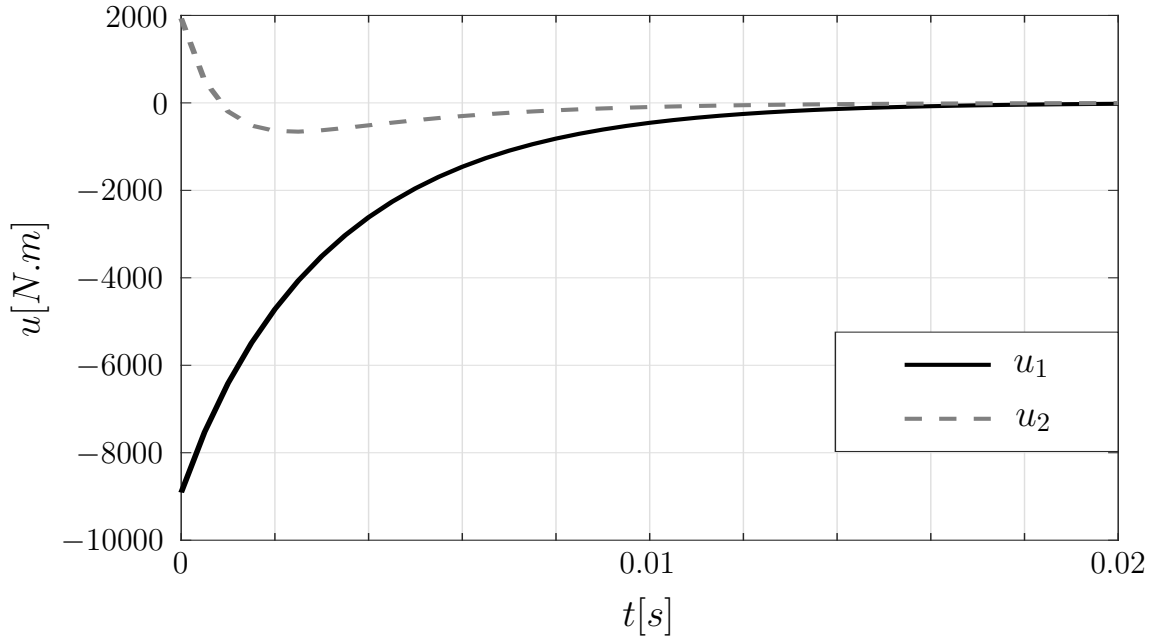

Source: the Author

The figures in the sequence show, in bold line, the contour slices of the ellipsoidal set $\mathcal{R}$ defined by the matrix P obtained in this numerical example. One should recall that this region $\mathcal{R}$ represents the set of admissible initial states, for which our synthesized controller is guaranteed to asymptotically stabilize the system trajectories within the specified exponential convergence rate criterion. The dashed lines shown the regions limited by the polytopes $\mathcal{X}$.

Figure 8 – Two dimensional slice of the estimated region of attraction with respect to the initial conditions $x_1(0)$ and $x_2(0)$, where $x_3 = x_4 = 0$ is considered.

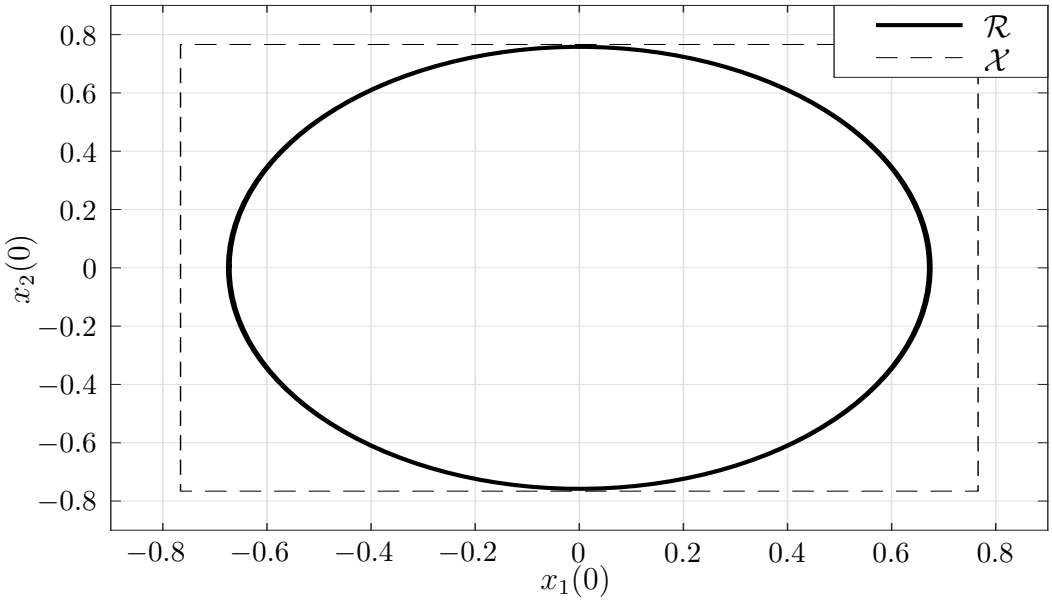

Source: the Author

Figure 9 – Two dimensional slice of the estimated region of attraction with respect to the initial conditions $x_3(0)$ and $x_4(0)$, where $x_1 = x_2 = 0$ is considered.

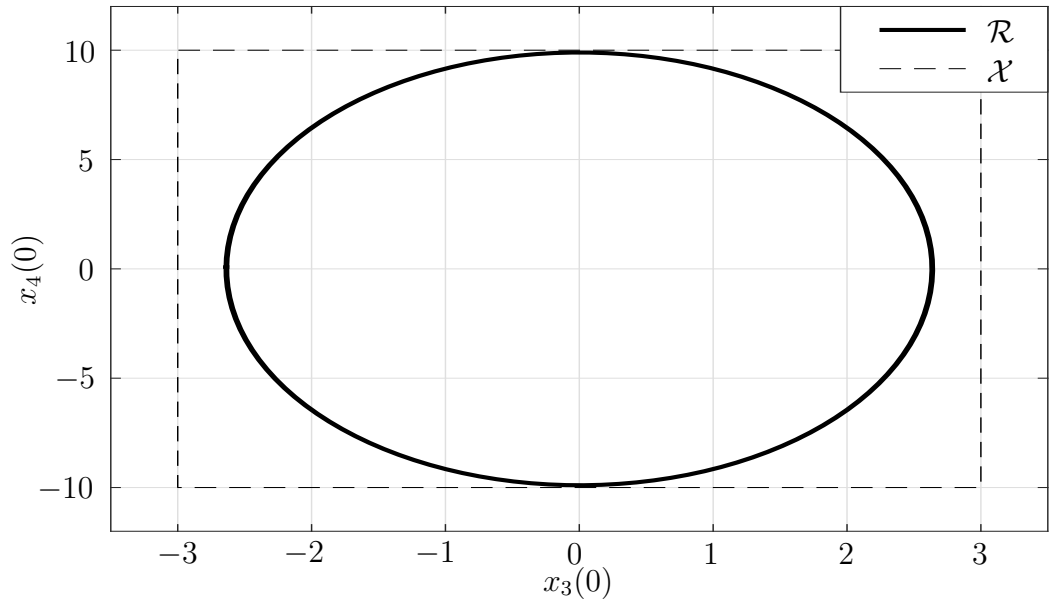

Source: the Author

Figure 10 – Two dimensional slice of the estimated region of attraction with respect to the initial conditions $x_1(0)$ and $x_3(0)$, where $x_2 = x_4 = 0$ is considered.

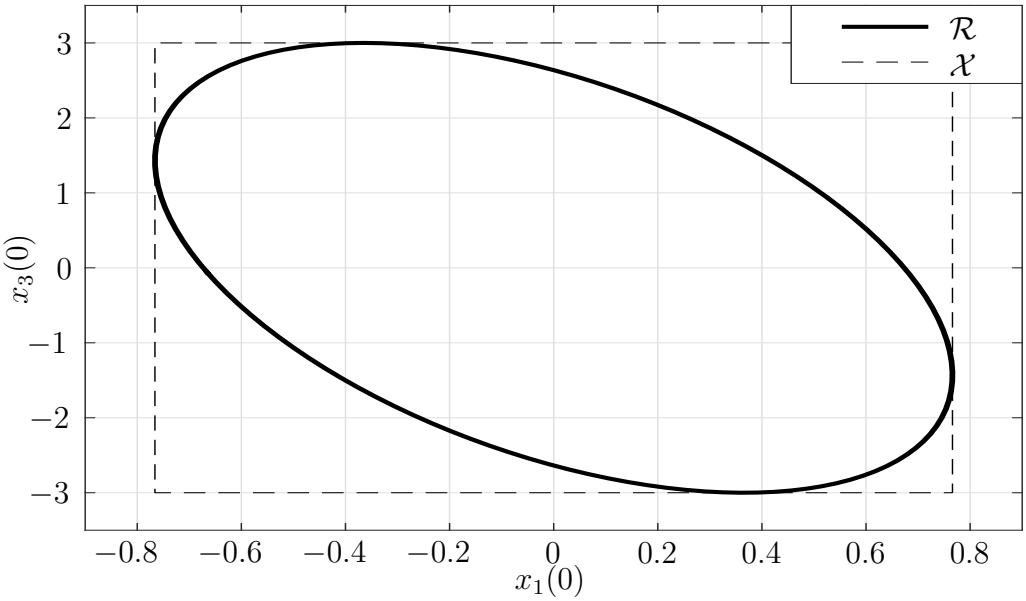

Source: the Author

Figure 11 – Two dimensional slice of the estimated region of attraction with respect to the initial conditions $x_2(0)$ and $x_4(0)$, where $x_1 = x_3 = 0$ is considered.

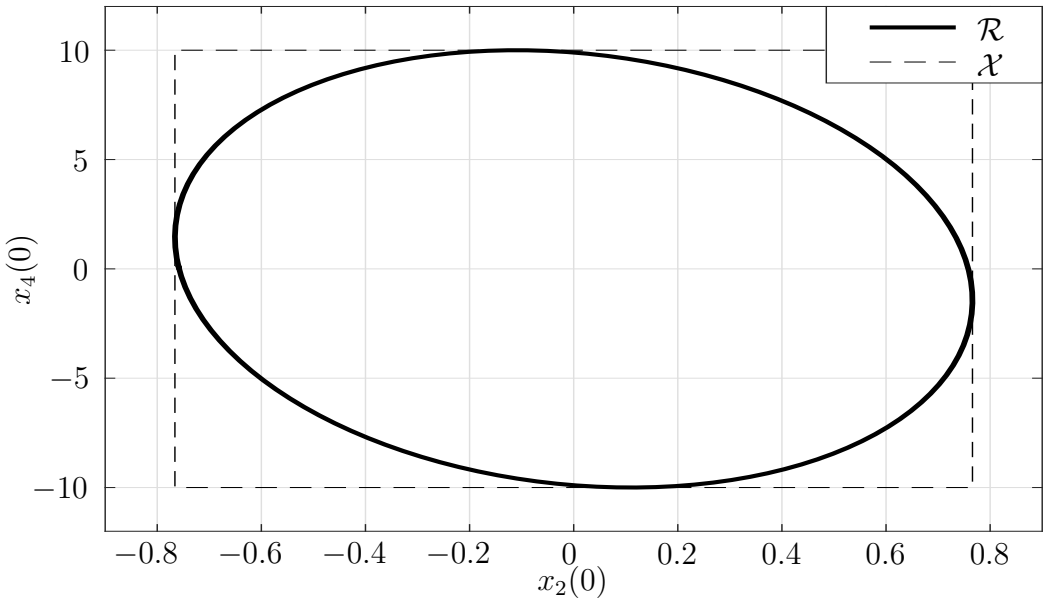

Source: the Author

Figure (12) show the initial condition adopted in the simulation. Once the initial conditions are within the region of attraction estimate $\mathcal{R}$, the convergence is guaranteed with an exponential decay rate given by λ. In the following figure, the "*" denotes the initial condition while the line denotes the trajectory of the simulated system.

Figure 12 – Trajectory of the simulated system.

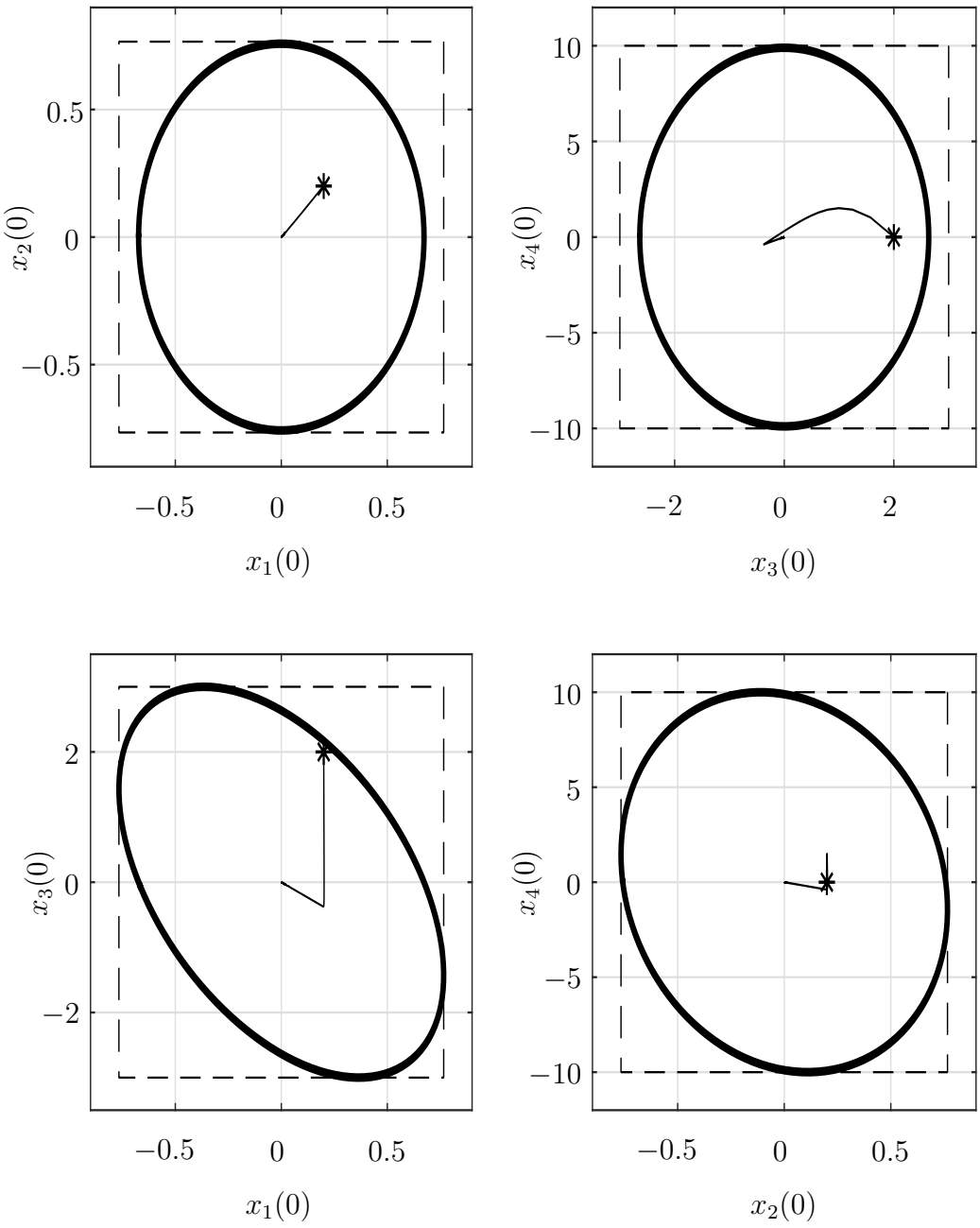

Source: the Author

To better understand the results presented by the figures above, Figure (13) presents the spatial trajectory of the manipulator viewed from above. Overlapping frames with an interval of 1 seconds between them, extracted from an animation. Time ranges from 0 to 8 seconds.

Figure 13 – Spatial trajectory of the manipulator.

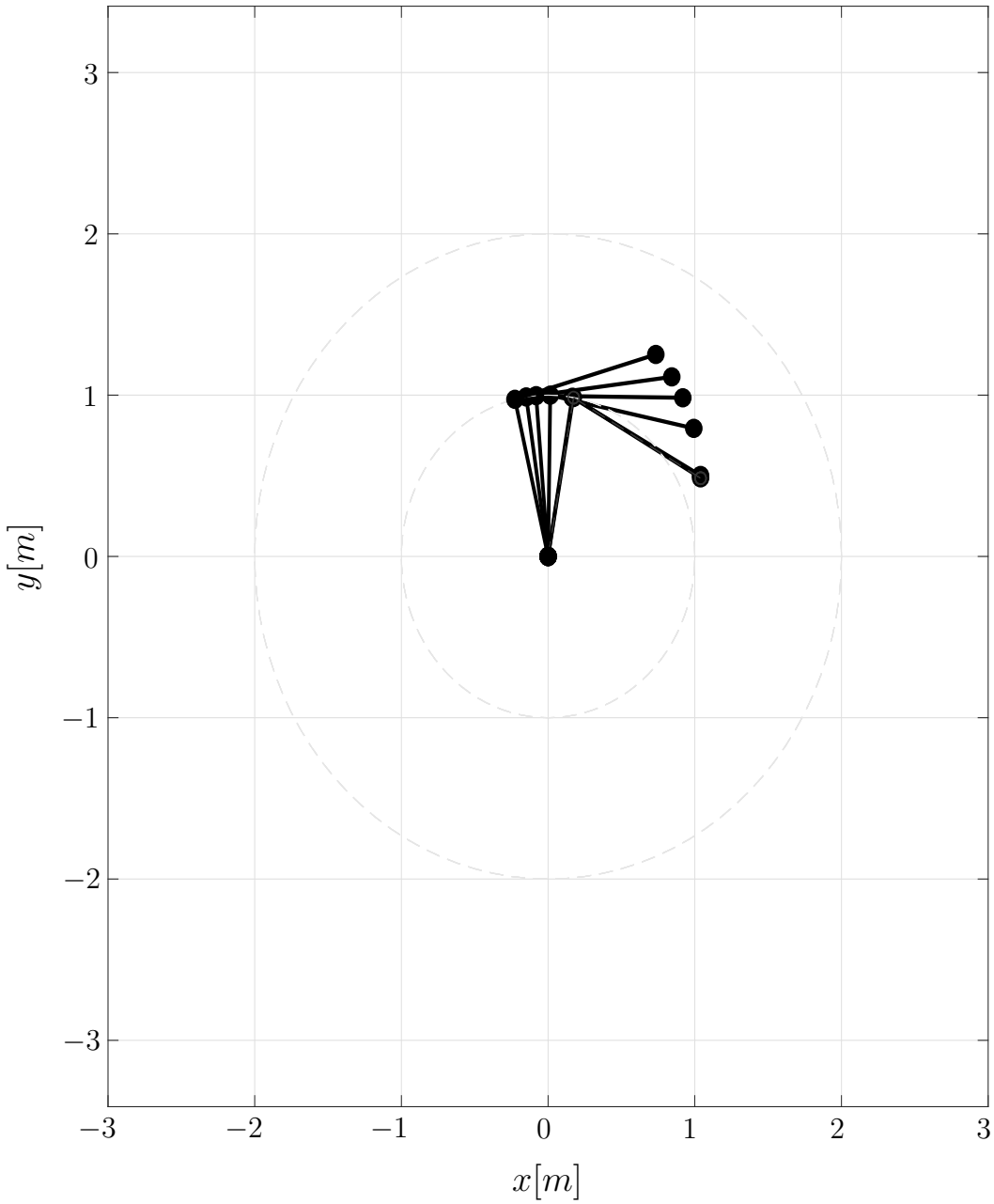

Source: the Author

Figures (14), (15), (16) and (17) are presented to exemplify the change of reference. Consider the same system presented above and assume that upon reaching the predetermined reference, a new reference is allowed. Regardless of reference changes stability is guaranteed as long as the system states are within the estimate of attraction region $\mathcal{R}$. The new target reference attitude angles were defined as $\theta_{r_1} = 90^\circ$ and $\theta_{r_2} = -90^\circ$ and since the last reference were set as $\theta_1(0) = 80^\circ$ and $\theta_2(0) = -110^\circ$, yielding the error $\theta_{e1} = -10^\circ$ and $\theta_{e2} = -20^\circ$ (which are equivalent to $x_1(0) = -0.0872$ and $x_2(0) = -0.1736$ in the quaternion error representation).

In Figure (14), it is possible to observe that after the reference is reached, a new reference is considered for the system, demonstrating system stability for different reference values. Figure (15) show the abrupt change of angular velocity due to the reference change considered.

Figure 14 – Time series of the error angles $\theta_e(t)$ yielded by the numerical simulation.

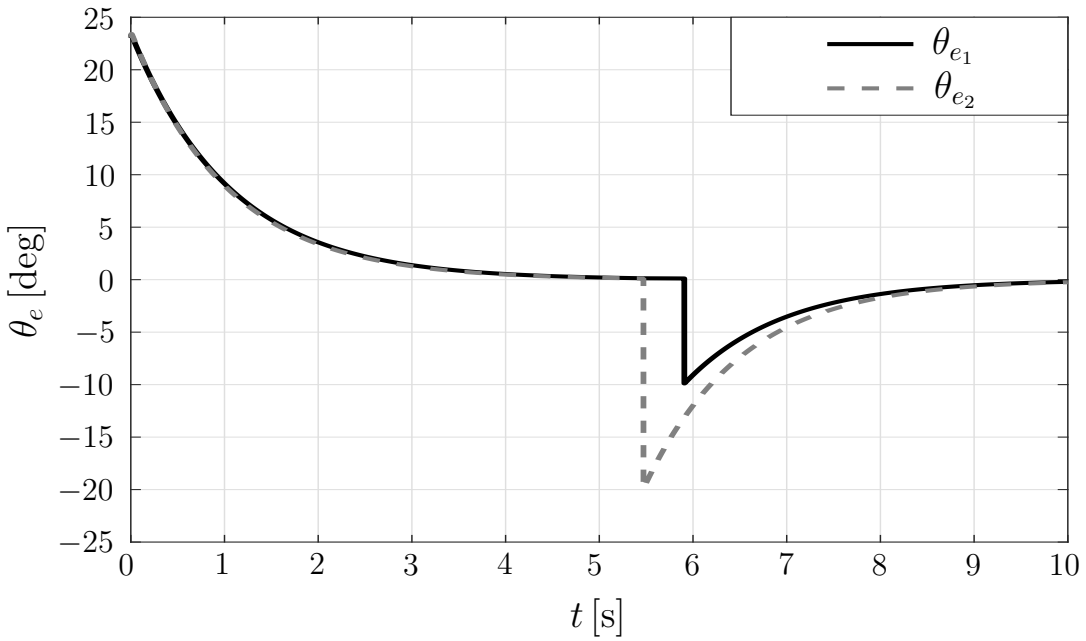

Source: the Author

Figure 15 – Time series of the angular velocities $\omega(t)$ yielded by the numerical simulation.

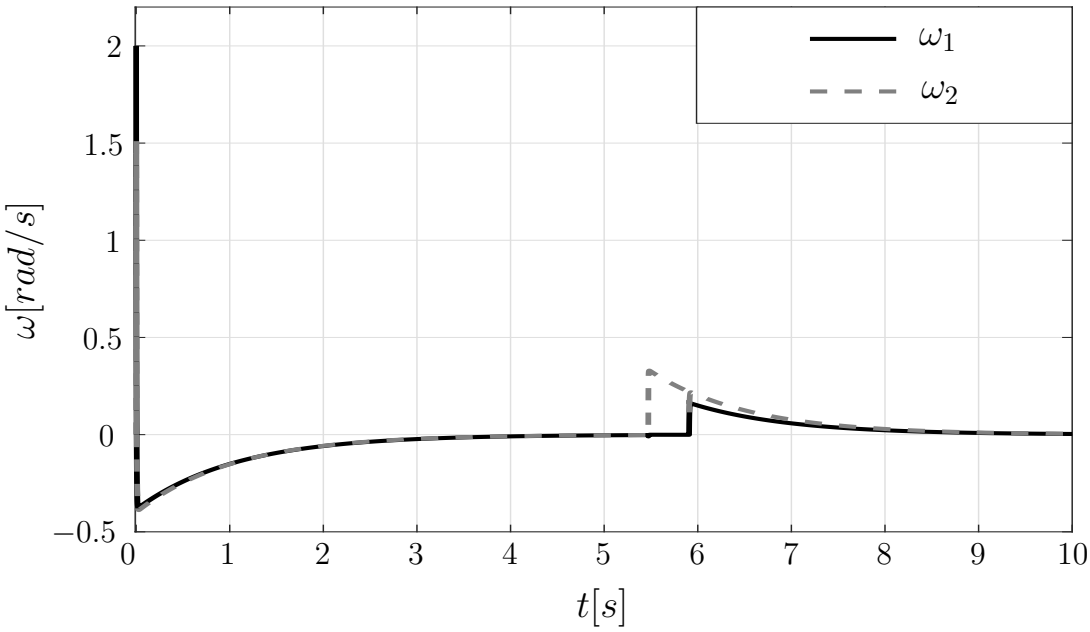

Source: the Author

Figure 16 – Time series of the link angles $\theta(t)$ yielded by the numerical simulation.

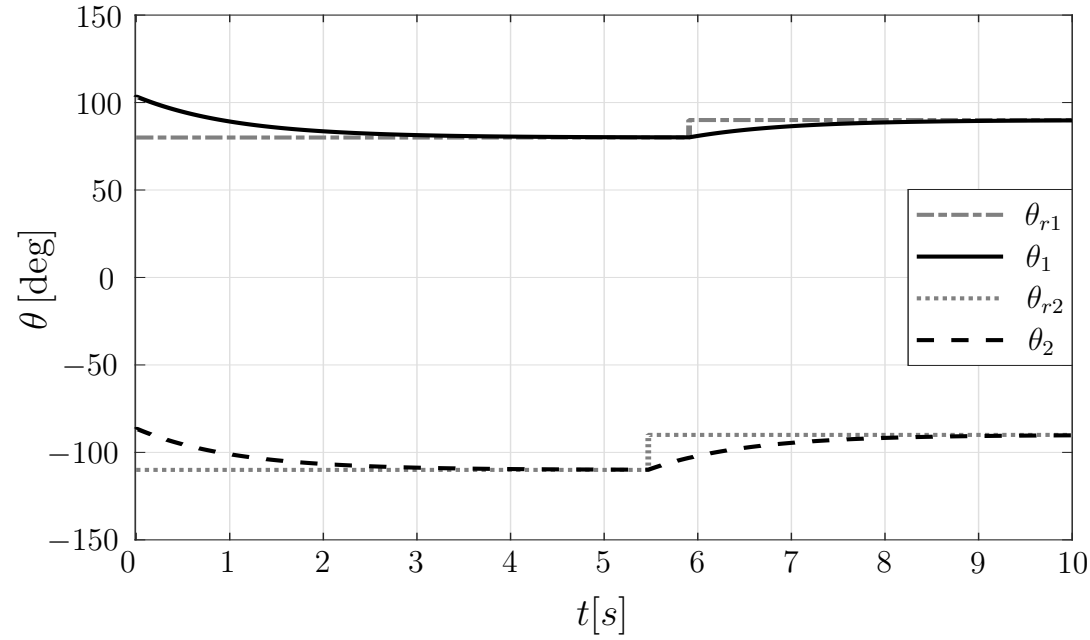

Source: the Author

Figure (17), exemplifies the choice of initial condition adopted in the simulation along with a second reference that belongs to the region $\mathcal{R}$. This fact assured the convergence with an exponential decay rate given by λ. In the following Figure, the "*" denotes the initial condition while the line denotes the trajectory of the simulated system. It can be noticed that after the trajectory reaches the origin, a new path begins, due to the reference given to the system.

Figure 17 – Trajectory of the simulated system with two references.

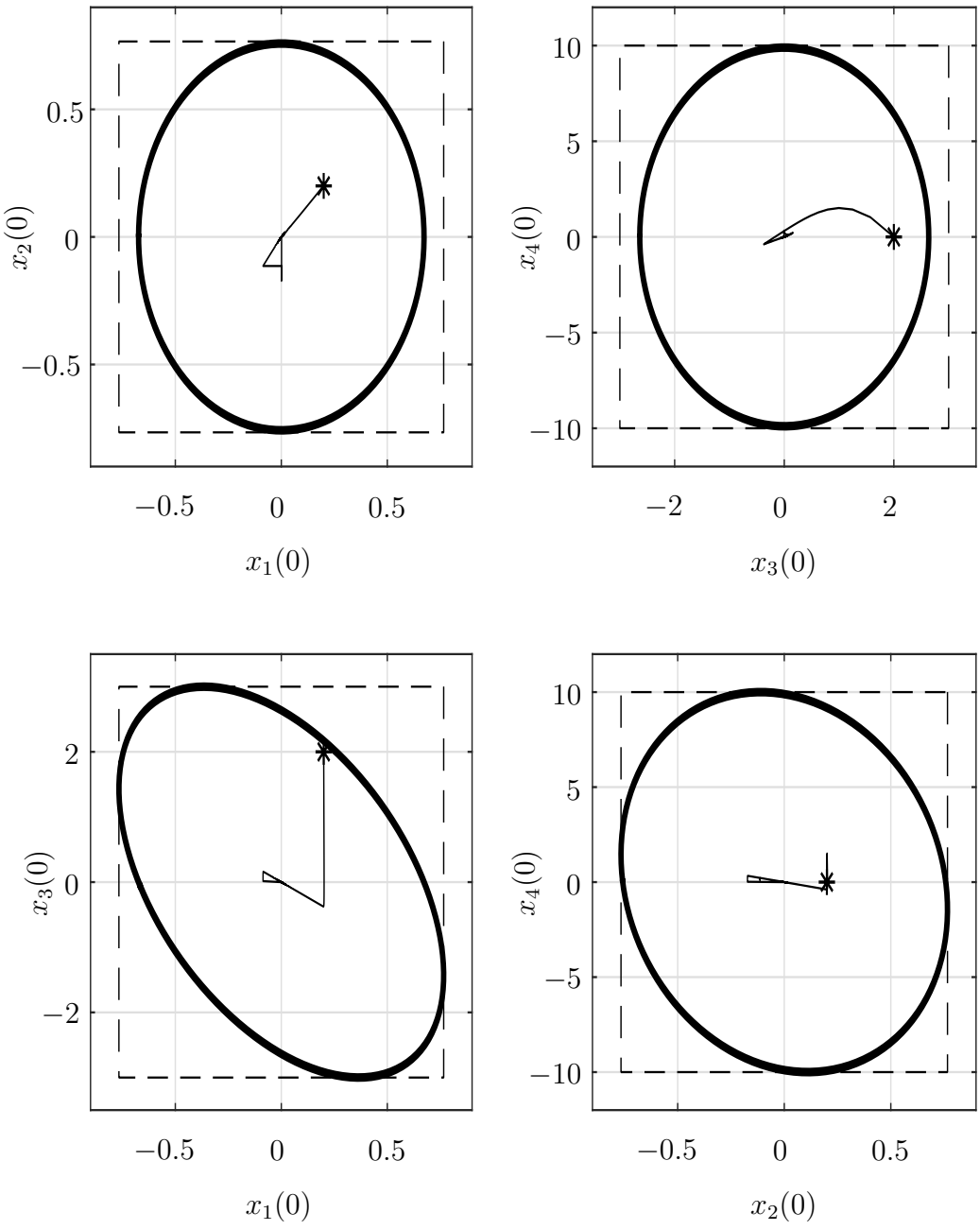

Source: the Author

4.2 Final Remarks

This chapter presented the framework introduced in Chapter 3. Also, the chapter brings a theorem in order to design a state feedback controller that ensures asymptotic stability. One should recall that this proposed design methodology is based on convex optimization subject to LMI contraints, which can be efficiently addressed by numerical solvers. By adhering to this strategy, this work provided a systematical method to add other nonlinearities to the controller, as an example the next chapter will present the controller synthesis with a saturation input constraint. The chapter then ends with the main results obtained by software simulation in order to illustrate the method itself.

5 Control Design subject to Input Saturation

This chapter provides a systematic design approach able to design a feedback controller for the robotic manipulator system presented in Section 2, where the proposed DAR developed in Section 3 will be explored in order to deal with the input saturation of the actuators, which is an inherent effect of every practical application. It is important to emphasize that this methodology will provide rigorous stability and performance guarantees, without resorting to any kind of linearization or approximation.

The robotic manipulator controller to be considered in here is a state-feedback law subject to saturation, i.e.

$$\begin{cases} u = & \text{sat}(\mu) \\ \mu = & Kx \end{cases}. \tag{104}$$

In this case, it follows that system (104) can be written as

$$\begin{cases} \dot{x} = (\mathbf{A}_1(\delta) + \mathbf{B}K)\, x + \mathbf{A_2}(x,\delta)\, \xi_a - \mathbf{B}\, \varphi(Kx) \\ 0 = (\mathbf{\Omega_1}(\delta) + \mathbf{\Omega_3}K)\, x + \mathbf{\Omega_2}(x,\delta)\, \xi_a - \mathbf{\Omega_3}\, \varphi(Kx) \end{cases}. \tag{105}$$

The following theorem is proposed in order to design the controller considering the input saturation effect. The theorem is adapted from (CASTRO, 2019) and the same exponential criterion presented in Definition 4.1 is also considered. It is important to notice that the input saturation signal is denoted by $\overline{u}_i$.

Theorem 5.1. *Suppose that there exist a symmetric matrix $\hat{P} \in \mathbb{R}^{4\times4}$, a diagonal matrix $\hat{T} \in \mathbb{R}^{2\times2}$ and generic matrices $\hat{L} \in \mathbb{R}^{6\times6}$ and $\hat{K}, \hat{G} \in \mathbb{R}^{2\times4}$ such that:*

$$\hat{P} > 0\,, \;\; \hat{T} > 0\,, \tag{106}$$

$$\begin{bmatrix} 1 & \alpha_k \hat{P} \\ \star & \hat{P} \end{bmatrix} > 0 \, \forall \, k = 1,2,3,4, \tag{107}$$

$$\begin{bmatrix} \overline{u}_i^2 & \hat{K}_{[i]} - \hat{G}_{[i]} \\ \star & \hat{P} \end{bmatrix} > 0 \, \forall \, i = 1,2, \tag{108}$$

$$\text{He}\left\{ \begin{bmatrix} \mathbf{A_1}(\delta)\hat{P} + \lambda\hat{P} + \mathbf{B}\hat{K} & \mathbf{A_2}(x,\delta)\hat{L} & -\mathbf{B}\hat{T} \\ \mathbf{\Omega_1}(\delta)\hat{P} + \mathbf{\Omega_3}\hat{K} & \mathbf{\Omega_2}(x,\delta)\hat{L} & -\mathbf{\Omega_3}\hat{T} \\ \hat{G} & 0 & -\hat{T} \end{bmatrix} \right\} < 0\,, \tag{109}$$

$\forall\,(x,\delta)\in\mathcal{V}(\mathcal{X})\times\mathcal{V}(\Delta)$. *Then the trajectories* $x(t)$ *of the closed-loop system* (105) *with* $K=\hat{K}\hat{P}^{-1}$ *exponentially approach the origin with decay rate greater than* λ *for every initial condition* $x(0)$ *in*

$$\mathcal{R}=\left\{x\in\mathbb{R}^4:x^{\mathsf{T}}Px\leq 1\right\},\;\; P\triangleq\hat{P}^{-1}\,. \tag{110}$$

Proof. Consider the Lyapunov candidate function

$$V(x)=x^{\mathsf{T}}Px\,, \tag{111}$$

where $P\in\mathbb{R}^{4\times 4}$ is a symmetric and positive-definite matrix as ensured by (107). By differentiating this function along the trajectories of system (105), one obtains

$$\dot{V}(x,\delta)=\mathrm{He}\{x^{\mathsf{T}}\begin{bmatrix}P(\mathbf{A_1}(\delta)+\mathbf{B}\hat{K}) & P\mathbf{A_2}(x,\delta) & -P\mathbf{B}\end{bmatrix}\zeta\}, \tag{112}$$

where ζ is defined as:

$$\zeta\triangleq\begin{bmatrix}x^{\mathsf{T}} & \xi_a^{\mathsf{T}} & \varphi^{\mathsf{T}}(Kx)\end{bmatrix}^{\mathsf{T}}. \tag{113}$$

Observe that, for any matrix $L\in\mathbb{R}^{6\times 6}$, the algebraic constraint in (105) implies that

$$0=\mathrm{He}\{\xi_a^{\mathsf{T}}\begin{bmatrix}L(\mathbf{\Omega_1}(\delta)+\mathbf{\Omega_3}\hat{K}) & L\mathbf{\Omega_2}(x,\delta) & -L\mathbf{\Omega_3}\end{bmatrix}\zeta\} \tag{114}$$

is true.

Consider the Lemma 2.5 for $n_x=4$, $n_u=2$ and assume that $x\in\mathcal{S}$, where $\mathcal{S}$ is the polyhedral set introduced in (20). In this case, for any diagonal and positive-definite $T\in\mathbb{R}^{2\times 2}$, relation (21) is verified, which is in turn equivalent to

$$\mathrm{He}\{\varphi^{\mathsf{T}}(Kx)\begin{bmatrix}TG & 0 & -T\end{bmatrix}\zeta\}\geq 0. \tag{115}$$

Now suppose that the following expression holds $\forall\,(x,\delta)\in\mathcal{X}\times\Delta$:

$$\begin{aligned}\mathrm{He}\Big\{&x^{\mathsf{T}}\begin{bmatrix}P(\mathbf{A_1}(\delta)+\mathbf{B}\hat{K}) & P\mathbf{A_2}(x,\delta) & -P\mathbf{B}\end{bmatrix}\zeta+\\ &\xi_a^{\mathsf{T}}\begin{bmatrix}L(\mathbf{\Omega_1}(\delta)+\mathbf{\Omega_3}\hat{K}) & L\mathbf{\Omega_2}(x,\delta) & -L\mathbf{\Omega_3}\end{bmatrix}\zeta+\\ &\varphi^{\mathsf{T}}(Kx)\begin{bmatrix}TG & 0 & -T\end{bmatrix}\zeta+x^{\mathsf{T}}\lambda P\,x\Big\}<0\,,\end{aligned} \tag{116}$$

relation that can be rewritten as

$$\mathrm{He}\{A\}\left\{\begin{bmatrix}P(\mathbf{A_1}(\delta)+\mathbf{B}\hat{K})+\lambda P & P\mathbf{A_2}(x,\delta) & -P\mathbf{B}\\ L(\mathbf{\Omega_1}(\delta)+\mathbf{\Omega_3}\hat{K}) & L\mathbf{\Omega_2}(x,\delta) & -L\mathbf{\Omega_3}\\ TG & 0 & -T\end{bmatrix}\right\}<0. \tag{117}$$

If (117) is verified then the derivative of the Lyapunov function (111) is negative-definite inside the domain $(\mathcal{X} \cap \mathcal{S}) \times \Delta$, i.e.

$$\dot{V}(x,\delta) < -2\lambda V(x) < 0 \,\forall\, x \in (\mathcal{X} \cap \mathcal{S}) - \{0\}\,,\, \forall\, \delta \in \Delta\,. \tag{118}$$

By considering a level set of the candidate Lyapunov function as an invariant domain of attraction estimate $\mathcal{R}$, for instance $\mathcal{R} = \{x \in \mathbb{R}^4 : x^\intercal P x \leq 1\}$, such that $\mathcal{R} \subset \mathcal{X}$ and $\mathcal{R} \subset \mathcal{S}$, the validity of Lemma 2.5 is assured.

Similarly to Chapter 4, based on the definition of $\mathcal{X}$ in (83), in order to ensure that $\mathcal{R} \subset \mathcal{X}$, it is necessary and sufficient to guarantee that $x^\intercal \alpha_k^\intercal \alpha_k\, x < x^\intercal P x \leq 1 \Leftrightarrow P - \alpha_k^\intercal \alpha_k > 0 \,\forall\, k = 1,2,3,4$.

Likewise, the inclusion condition $\mathcal{R} \subset \mathcal{S}$ holds if and only if

$$x^\intercal (K_{[j]} - G_{[j]})^\intercal (K_{[j]} - G_{[j]})\, x < x^\intercal P x^\intercal \leq 1 \Leftrightarrow \tag{119}$$

$$P - (K_{[j]} - G_{[j]})^\intercal (K_{[j]} - G_{[j]}) > 0 \Leftrightarrow \tag{120}$$

$$\begin{bmatrix} 1 & K_{[j]} - G_{[j]} \\ \star & P \end{bmatrix} > 0 \,\forall\, j = 1,2\,. \tag{121}$$

Consequently, if conditions the conditions $P > 0$, $T > 0$, (121) and (117) are satisfied, the trajectories $x(t)$ of the closed-loop system (105) asymptotically approach the origin for every initial condition $x(0) \in \mathcal{R}$. The proof regarding the exponential convergence criterion, from Definition 4.1, is identical to the proof of Theorem 4.1.

By then pre- and post-multiplying the matrix inequalities $P > 0$, $T > 0$, (121) and (117) respectively by P^{-1}, T^{-1}, $\mathrm{diag}\{1, P^{-1}\}$, $\mathrm{diag}\{1, P^{-1}\}$, $\mathrm{diag}\{P^{-1}, L^{-1}, T^{-1}\}$, and their transposes, one should finally obtain the conditions presented in (106), (107), (108) and (109) when considering the change of variables $\hat{P} \triangleq P^{-1}$, $\hat{K} \triangleq KP^{-1}$, $\hat{G} \triangleq RP^{-1}$, $\hat{L} \triangleq L^{\intercal -1}$ and $\hat{T} \triangleq T^{-1}$.

To conclude the proof, if the LMI (109) is satisfied for (x,δ) at the vertices $\mathcal{V}(\mathcal{X}) \times \mathcal{V}(\Delta)$, by convexity they are also satisfied $\forall\, (x,\delta) \in \mathcal{X} \times \Delta$. □

In order to maximize the size of the domain of attraction estimate $\mathcal{R}$, as explained in the previous chapter, one can minimize the trace of $\hat{P}^{-1}$ subject to the LMIs from Theorem 5.1. The optimal control design which maximizes the domain of attraction estimate $\mathcal{R}$ can therefore be synthesized by the following convex optimization:

$$\begin{aligned} &\underset{N,\hat{P},\hat{T},\hat{L},\hat{K},\hat{G}}{\text{minimize}} \quad \mathrm{tr}(N) \\ &\text{subject to} \quad (106),(107),(108),(109) \begin{bmatrix} N & I \\ \star & \hat{P} \end{bmatrix} > 0. \end{aligned} \tag{122}$$

5.1 Numerical Example

Similarly to Chapter 4 this section presents the result obtained by numerical simulation using MATLAB R2012b software and its native LMILAB toolbox. Here also, an ideal two-link manipulator was considered where the constructive parameters are given in Table 3

Table 3 – Physical parameters of the robotic manipulator example.

Parameter	Value
m_1	$10\,\mathrm{kg}$
m_2	$1\,\mathrm{kg}$
ℓ_1	$1\,\mathrm{m}$
ℓ_2	$1\,\mathrm{m}$
$\overline{u}_1$	$10^3\,\mathrm{Nm}$
$\overline{u}_2$	$10^2\,\mathrm{Nm}$

Table 4 – Control design parameters.

Parameter	Value
$\overline{\theta}_{e_1}$	100°
$\overline{\theta}_{e_2}$	100°
$\overline{\omega}_1$	$3\,\mathrm{rad/s}$
$\overline{\omega}_2$	$10\,\mathrm{rad/s}$
λ	0.6
θ_{r1}	80°
θ_{r2}	-110°

Towards employing the proposed control synthesis approach, the target domain of interest $\mathcal{X}$ and the minimum exponential convergence rate criterion, as defined in (4.1) were defined as shown in Table 4. Given these setup parameters, the proposed convex optimization problem (122) yielded the feedback matrix

$$K = \begin{bmatrix} -966.62 & 8.6760 & -495.81 & 30.852 \\ 233.49 & -162.96 & 125.78 & -54.387 \end{bmatrix}, \tag{123}$$

in which case the domain of attraction estimate (110) is defined with

$$P = \begin{bmatrix} 2.2471 & 0.0009 & 0.2821 & 0.0004 \\ 0.0009 & 1.7517 & -0.0001 & 0.0221 \\ 0.2821 & -0.0001 & 0.1465 & 0.0001 \\ 0.0004 & 0.0221 & 0.0001 & 0.0103 \end{bmatrix}, \tag{124}$$

where $\mathrm{tr}(P) = 4.1556$.

Similarly to chapter 4, Figure (18) and Figure (19) show the time series produced by a numerical simulation of the closed-loop system but adding the input saturation effect. The

target reference attitude angles were defined as $\theta_{r_1} = 80^\circ$ and $\theta_{r_2} = -100^\circ$ and the initial manipulator angles as $\theta_1(0) = 103.07^\circ$ and $\theta_2(0) = -86.93^\circ$, yielding the initial errors $\theta_{e_1}(0) = \theta_{e_2}(0) = 23.06^\circ$ for both joint angles. In turn, the initial joint angular velocities were considered as $\omega_1(0) = x_3(0) = 2\,\mathrm{rad/s}$ and $\omega_2(0) = x_4(0) = 0\,\mathrm{rad/s}$. This system initial state is marginally close to the border of the domain of attraction estimate $\mathcal{R}$, also the initial state was chosen to be in the saturated region $\mathcal{U}$. As we can see the states exponentially converge to the origin.

Figure 18 – Time series of the error angles $\theta_e(t)$ yielded by the numerical simulation.

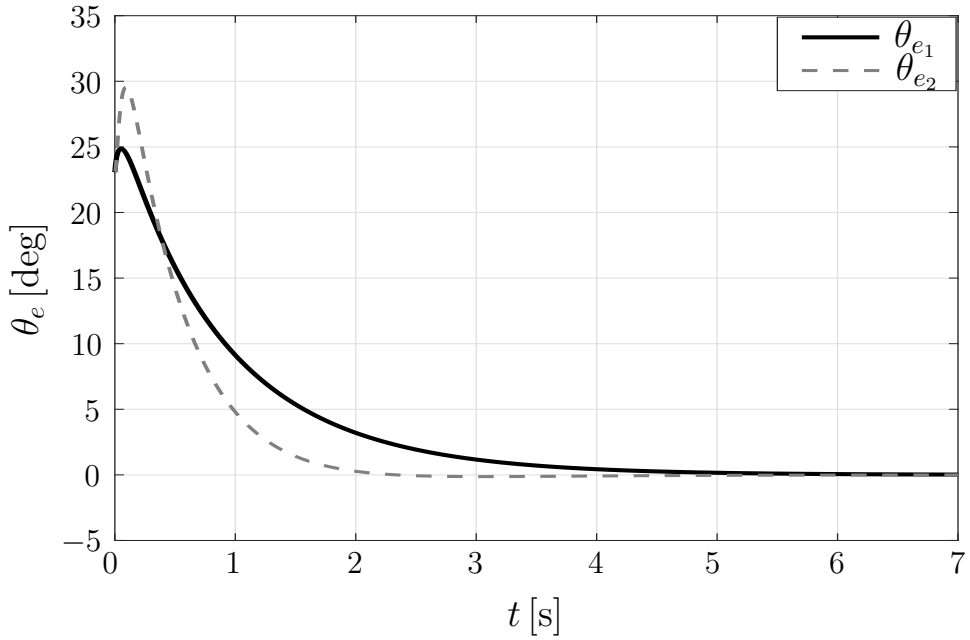

Source: the Author.

Figure 19 – Time series of the error angles $\omega(t)$ yielded by the numerical simulation.

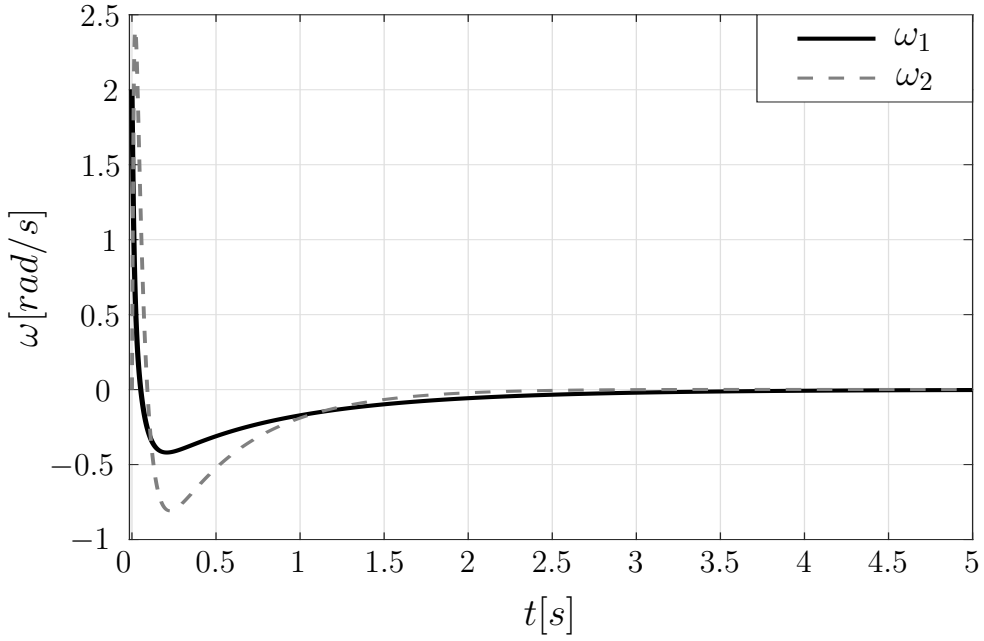

Source: the Author.

Even though the input saturation effect is now included in the system, Figure (20) shows that the proposed design method ensures a response where the angles θ_i exponentially converge to the reference θ_{ri} within the same decay rate that was presented in Table 4.

Figure 20 – Time series of the link angles $\theta(t)$ yielded by the numerical simulation.

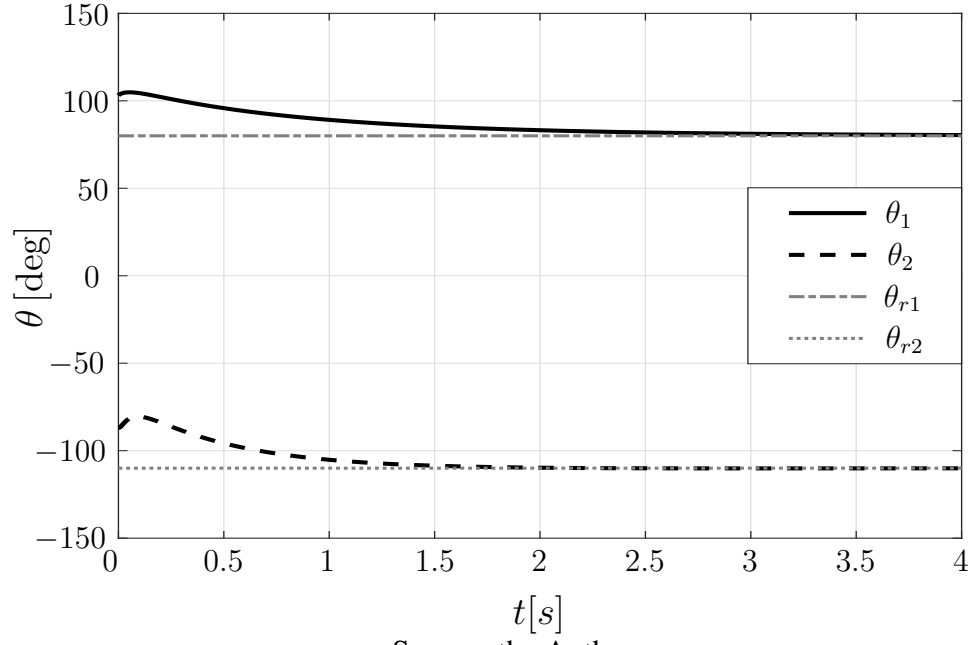

Source: the Author.

Figure (21) shows time series of the control signal $u(t)$. The top figure shows that both control signals rapidly converge. The bottom plot is the zoom in of the top figure showing the saturated period in control signals. The initial condition was chosen so that both input signals were in the saturated region at the same time.

Figure 21 – Time series of the control signal $u(t)$ yielded by the numerical simulation.

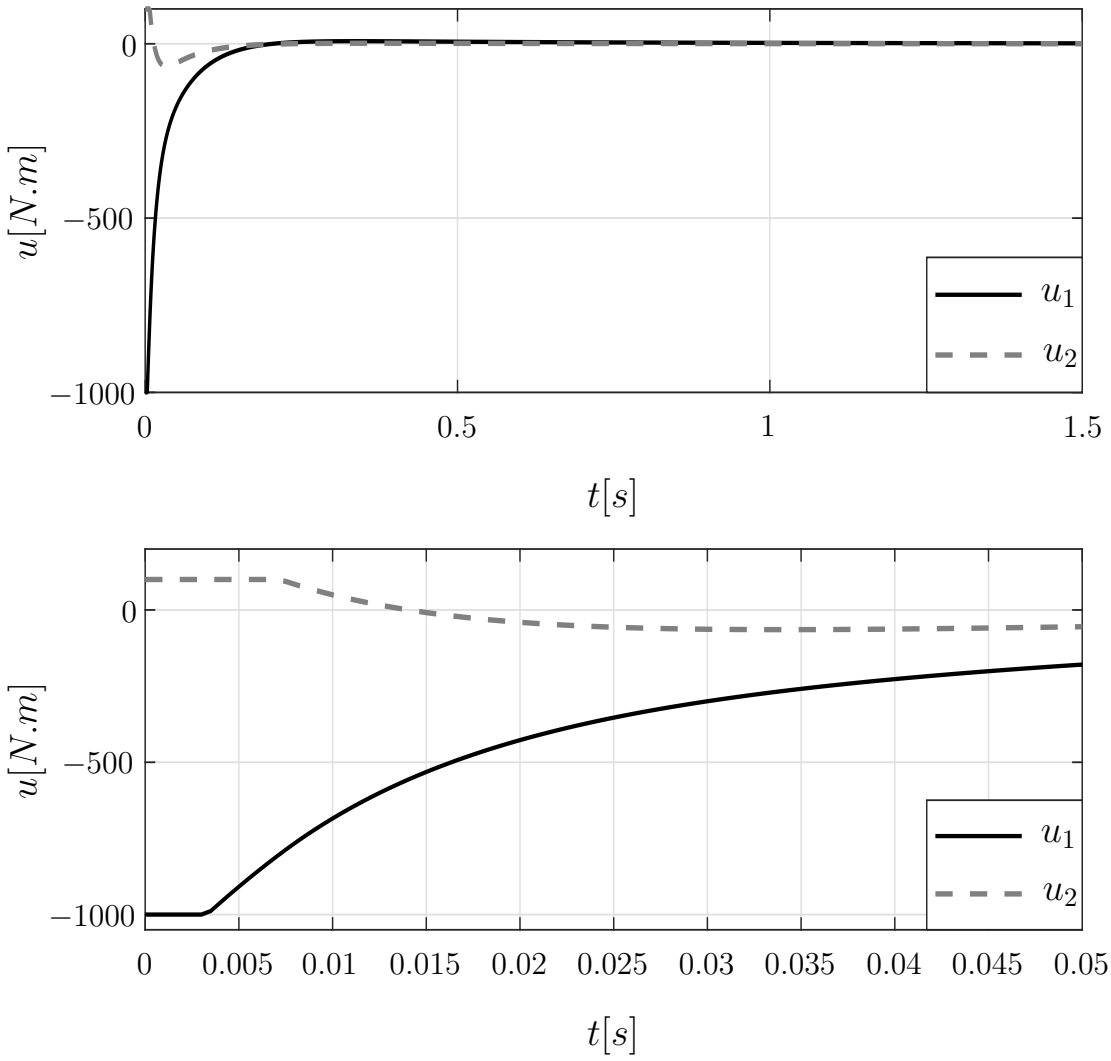

Source: the Author.

The Figures (22) to (25) show, in bold line, the contour slices of the ellipsoidal set $\mathcal{R}$ defined by the matrix P. The region $\mathcal{R}$ represents the set of admissible initial states, for which our synthesized controller is guaranteed to asymptotically stabilize the system trajectories within the specified exponential convergence rate criterion λ. Also, the dashed-dotted and dotted bars denote the control input saturation borderlines, where $\mathcal{U}_1 = \overline{u}_1$ and $\mathcal{U}_2 = \overline{u}_2$ respectively. So, to work in the saturation region of the actuators the initial conditions have to be chosen outside of both regions $\mathcal{U}_1$ and $\mathcal{U}_2$. To exemplify, any initial condition chosen in Figure (22) has no impact in the saturation of the link 1 actuator. On the other hand, initial conditions chosen in

Figure (23) can impact the saturation of both actuators. The results illustrate that the proposed method is capable of providing stability and performance guarantees even for initial conditions that saturate both input signals.

Figure 22 – Two dimensional projection of the estimated region of attraction considering x_1 and x_2 with $x_3 = x_4 = 0$.

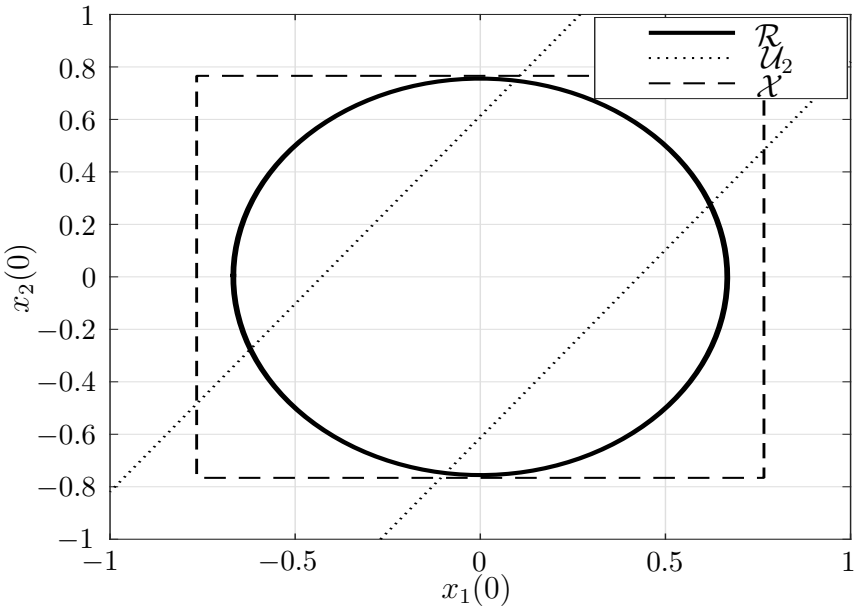

Source: the Author.

Figure 23 – Two dimensional projection of the estimated region of attraction considering x_3 and x_4 with $x_1 = x_2 = 0$.

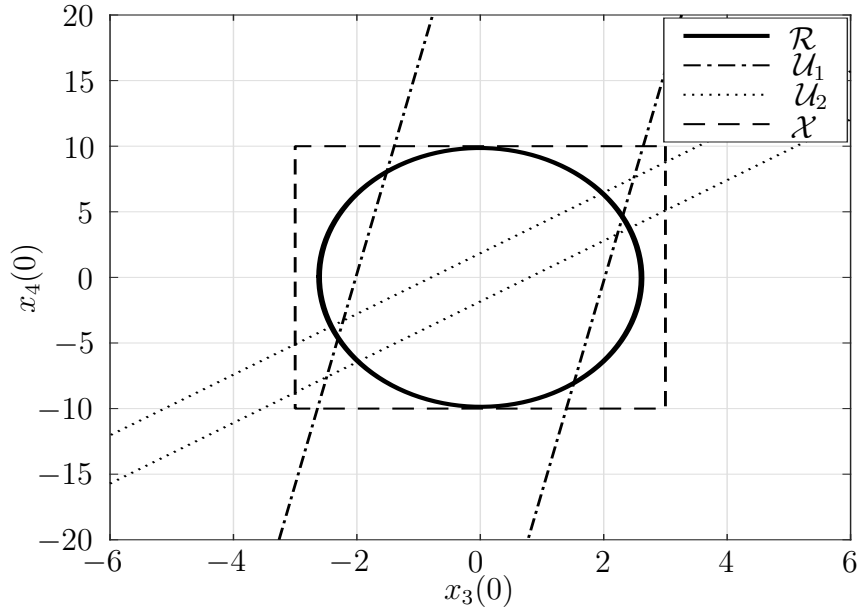

Source: the Author.

Figure 24 – Two dimensional projection of the estimated region of attraction considering x_1 and x_3 with $x_2 = x_4 = 0$.

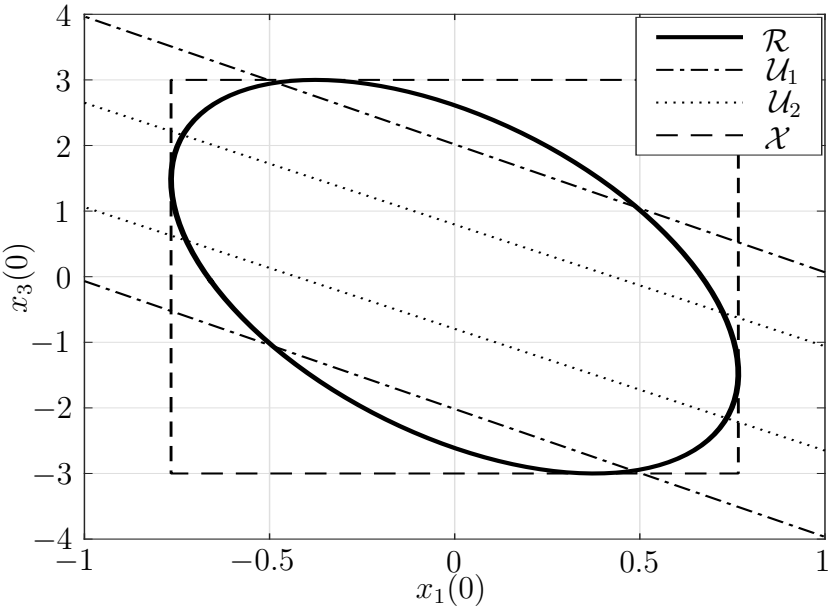

Source: the Author.

Figure 25 – Two dimensional projection of the estimated region of attraction considering x_2 and x_4 with $x_1 = x_3 = 0$.

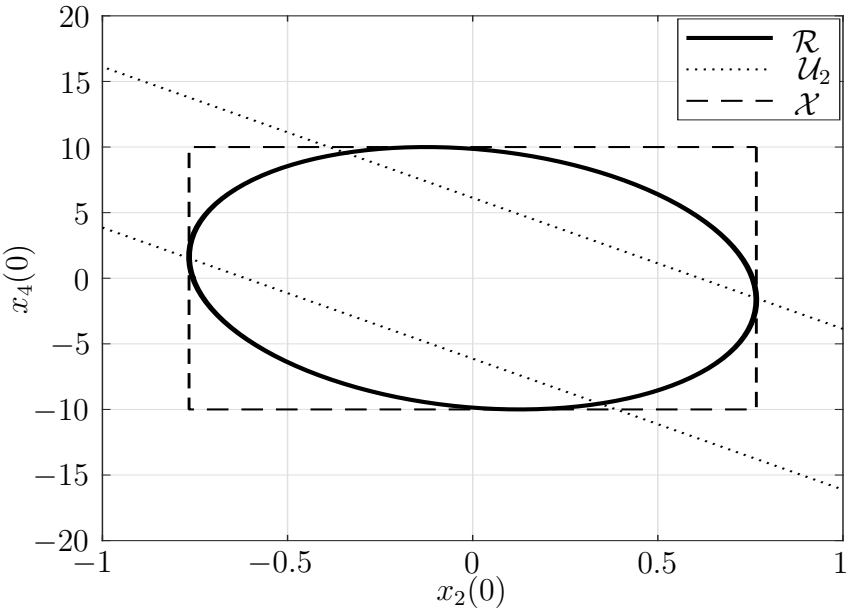

Source: the Author.

Exemplification of the initial condition that saturate both actuators adopted in the simulation are presented in Figure (26). The initial condition is inside the region $\mathcal{R}$, this fact assured the convergence with an exponential decay rate given by λ. Also, it can be noticed that the initial conditions are outside of both regions $\mathcal{U}$ in the bottom left image, meaning that the chosen initial conditions are in the saturation region of the actuators. In the following Figure, the "*"

denotes the initial condition while the line denotes the trajectory of the simulated system.

Figure 26 – Trajectory of planar manipulator subject to input saturate in actuators.

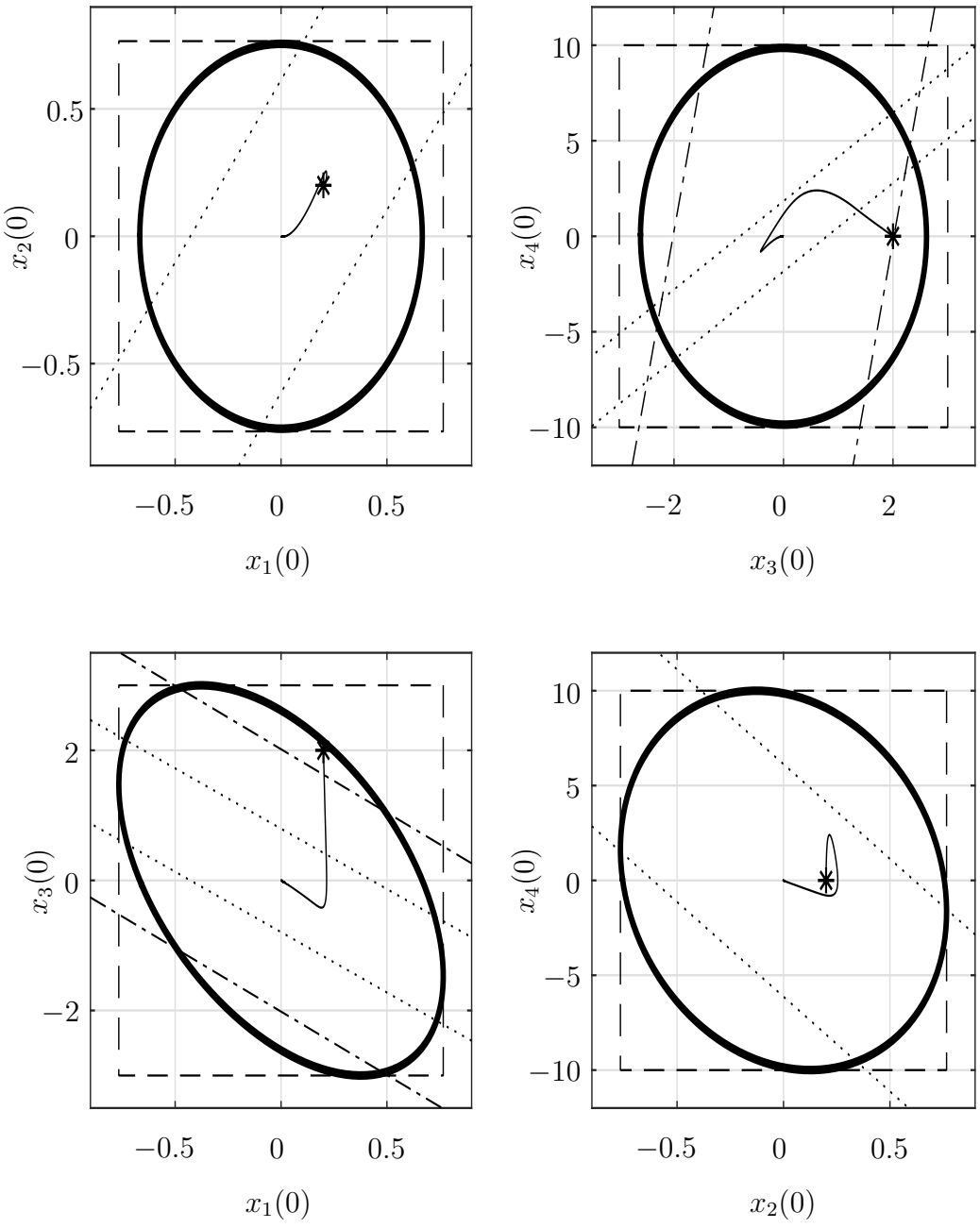

Source: the Author

5.2 Final Remarks

This chapter brought the addition of input saturation effect into the controller design problem in order to illustrate the extensibility of the preliminary methodology present in Chapter 4. The inclusion of this additional non-linearity is addressed by a new theorem that allows to synthesize the feedback gains by an optimization problem subject to new LMIs constraints. Finally, the chapter brings a numerical example to illustrate the results obtained via software simulation along with the main results.

6 Conclusion and Perspectives

This chapter brings an overview of the research highlighting the fulfillment of the established objectives and the main contribution. The perspective for related future works is also exposed afterward.

6.1 Overview of the Dissertation

The overall objective of this dissertation was to explore the usage of the differential-algebraic representation to design state feedback controllers for robotic manipulator systems. In this dissertation, theoretical results have been obtained considering a 2-link manipulator in quaternion-bases.

Chapter 3 introduced the proposed framework used to represent a two-link manipulator model. Then, the text presents the descriptor representation useful to avoid highly complex nonlinearities along with the fundamental methodology to accommodate the system in the differential-algebraic representation. Afterwards, Chapter 4 presented the theorem proposed to solve the optimization problems subject to LMIs constraints leading to a state feedback controller design that assures the stability and performance conditions. Then, the main results were presented by a numerical example via software simulation. Chapter 5 extends this approach by adding input saturation conditions to the controller design, where a new theorem is proposed to ensure the exponential convergence of the robot attitude error. This chapter has also illustrated the methodology via software simulation.

6.2 Future Perspectives

Aiming to expand the study of the proposed robotic manipulator control design framework, the next step would be the addition of gravity to the 2-link manipulator system. In order to do that, controllers with integral action would be a suggestion. Furthermore, a static anti-windup method would be suggested (GOMES DA SILVA JR et al., 2014) and subsequently extended to dynamics anti-windup design as proposed in (GOMES DA SILVA JR; LONGHI; OLIVEIRA, 2016) in order to improve the controller with integral action.

To achieve a less conservative region of attraction when compared to the one shown in this study, some approaches can be considered, such as non-quadratic Lyapunov functions or Linear annihilators. With regards to input saturation, the application of feedback linearization control that considers the saturation nonlinearity could be considered (KHALIL, 2002). Also, a nonlinear feedback control developed such as proposed in (CHEN et al., 2003; KHALIL, 2008)

could be an inspiration to work similarly with the addition of the DAR nonlinear vector to the control law that would add an extra degree of freedom for the synthesis optimization problem. Furthermore, gain-scheduling approaches can be considered, such as presented in (ZHANG et al., 2016; ZHANG; WANG, 2015) and H_∞ (RIZVI; LIN, 2018; MAO et al., 2018).

Output regulation methods can be studied in order to provide disturbance rejection when the manipulator is subject to exogenous forces due to end effector load or gravity. (ISIDORI; MARCONI; SERRANI, 2012). Beyond these, an effort to represent the system as closely as possible to a practical context would be accomplished by extending the methodology to a 6-degree of freedom system aiming to apply this control strategy along with the improvements presented above in a real manipulator to investigate the reliability of the presented framework.

Bibliography

BELOV, M. P.; KHOA, T. D.; TRUONG, D. D. Bldc of robotic manipulators with neural torque compensator based optimal robust control. In: IEEE. *2019 IEEE Conference of Russian Young Researchers in Electrical and Electronic Engineering (EIConRus)*. [S.l.], 2019. p. 437–441. Cited on page 21.

BOYD, S. et al. *Linear matrix inequalities in system and control theory*. [S.l.]: Society for Industrial and Applied Mathematics, 1994. (SIAM studies in applied mathematics). ISBN 9780898714852. Cited on page 27.

BURGNER-KAHRS, J.; RUCKER, D. C.; CHOSET, H. Continuum robots for medical applications: A survey. *IEEE Transactions on Robotics*, IEEE, v. 31, n. 6, p. 1261–1280, 2015. Cited on page 21.

CASTRO, R. S. *Output regulation of rational nonlinear systems with input saturation*. Tese (Doutorado) — Escola de Engenharia, 2019. Programa de Pós-Graduação em Engenharia Elétrica. Cited 3 times on pages 22, 45, and 61.

CHEN, B. M. et al. Composite nonlinear feedback control for linear systems with input saturation: Theory and an application. *IEEE Transactions on automatic control*, IEEE, v. 48, n. 3, p. 427–439, 2003. Cited on page 73.

CHEN, X. L. H. Piecewise control strategy for a planar four-link underactuated manipulator with friction. 2018. Cited on page 21.

CHERUBINI, A. et al. Collaborative manufacturing with physical human–robot interaction. *Robotics and Computer-Integrated Manufacturing*, Elsevier, v. 40, p. 1–13, 2016. Cited on page 21.

COSTA FABIAN A. LARA-MOLINA, A. A. C. J. e. E. T. T. L. Robust control of computed torque for manipulators. *IEEE LATIN AMERICA TRANSACTIONS, VOL. 16, NO. 2*, 2018. Cited on page 21.

COUTINHO, D. et al. Stability analysis and control of a class of differential-algebraic nonlinear systems. *International Journal of Robust and Nonlinear Control*, Wiley Online Library, v. 14, n. 16, p. 1301–1326, 2004. Cited on page 22.

COUTINHO, D. F.; GOMES DA SILVA JR, J. M. Estimating the region of attraction of nonlinear control systems with saturating actuators. In: IEEE. *2007 American Control Conference*. [S.l.], 2007. p. 4715–4720. Cited on page 22.

DIEBEL, J. Representing attitude: Euler angles, unit quaternions, and rotation vectors. *Matrix*, v. 58, n. 15-16, p. 1–35, 2006. Cited on page 36.

GENG, J.; ARAKELIAN, V. Design of partially balanced planar 5r symmetrical parallel manipulators via an optimal motion planning. In: SPRINGER. *IFToMM World Congress on Mechanism and Machine Science*. [S.l.], 2019. p. 2211–2220. Cited on page 21.

GOMES DA SILVA JR, J. M.; LONGHI, M. B.; OLIVEIRA, M. Z. Dynamic anti-windup design for a class of nonlinear systems. *International Journal of Control*, Taylor & Francis, v. 89, n. 12, p. 2406–2419, 2016. Cited on page 73.

GOMES DA SILVA JR, J. M. et al. Static anti-windup design for a class of nonlinear systems. *International Journal of Robust and Nonlinear Control*, Wiley Online Library, v. 24, n. 5, p. 793–810, 2014. Cited on page 73.

GOMES DA SILVA JR, J. M.; TARBOURIECH, S. Antiwindup design with guaranteed regions of stability: an lmi-based approach. *IEEE Transactions on Automatic Control*, IEEE, v. 50, n. 1, p. 106–111, 2005. Cited on page 27.

GUSNGZHENG WANG XUESONG, X. Y. P. Study on fuzzy pd control of planar two-link flexible manipulator. 2002. Cited on page 21.

HAMILTON, W. R. Xi. on quaternions; or on a new system of imaginaries in algebra. *The London, Edinburgh, and Dublin Philosophical Magazine and Journal of Science*, Taylor & Francis, v. 33, n. 219, p. 58–60, 1848. Cited on page 36.

IFR. *Robots double worldwide by 2020*. 2017. Disponível em: <https://ifr.org/ifr-press-releases/news/robots-double-worldwide-by-2020>. Cited on page 21.

ISIDORI, A.; MARCONI, L.; SERRANI, A. *Robust autonomous guidance: an internal model approach*. [S.l.]: Springer Science & Business Media, 2012. Cited on page 74.

KALI, M. S. Y. Dynamics formulation and motion control of a planar parallel manipulator. *Proceedings of the 3rd RSI International Conference on Robotics and Mechatronics, Iran*, 2015. Cited on page 21.

KALI, M. S. Y. Sliding mode with time delay control for mimo nonlinear systems with unknown dynamics. 2015. Cited on page 21.

KHALIL, H. *Nonlinear Systems*. [S.l.]: Prentice Hall, 2002. (Pearson Education). ISBN 9780130673893. Cited 3 times on pages 25, 26, and 73.

KHALIL, H. K. High-gain observers in nonlinear feedback control. In: IEEE. *2008 International Conference on Control, Automation and Systems*. [S.l.], 2008. p. xlvii–lvii. Cited on page 73.

KUIPERS, J. B. et al. *Quaternions and rotation sequences*. [S.l.]: Princeton university press Princeton, 1999. v. 66. Cited 2 times on pages 36 and 41.

LARA-MOLINA, F. A. et al. Robust generalized predictive control of the orthoglide robot. *Industrial Robot: An International Journal*, Emerald Group Publishing Limited, v. 41, n. 3, p. 275–285, 2014. Cited on page 21.

MAO, Q. et al. Attitude controller design for reusable launch vehicles during reentry phase via compound adaptive fuzzy h-infinity control. *Aerospace Science and Technology*, Elsevier, v. 72, p. 36–48, 2018. Cited on page 74.

RAHMANI, B.; BELKHEIRI, M. Robust adaptive control of robotic manipulators using neural networks : Application to a two link planar robot. *8th International Conference on Modelling, Identification and Control (ICMIC-2016) Algiers, Algeria*, 2016. Cited on page 21.

RIZVI, S. A. A.; LIN, Z. Output feedback q-learning for discrete-time linear zero-sum games with application to the h-infinity control. *Automatica*, Elsevier, v. 95, p. 213–221, 2018. Cited on page 74.

RUS, D.; TOLLEY, M. T. Design, fabrication and control of soft robots. *Nature*, Nature Publishing Group, v. 521, n. 7553, p. 467, 2015. Cited on page 21.

SALTON, A. T. et al. Semidefinite programming solution to the spacecraft analysis and control problem. *IFAC-PapersOnLine*, Elsevier, v. 50, n. 1, p. 3959–3964, 2017. Cited 3 times on pages 22, 37, and 41.

SICILIANO, B.; KHATIB, O. *Springer handbook of robotics*. [S.l.]: Springer, 2016. Cited on page 21.

SPONG, M. W. et al. *Robot modeling and control*. [S.l.: s.n.], 2006. Cited 2 times on pages 21 and 30.

TARBOURIECH, S. et al. *Stability and stabilization of linear systems with saturating actuators*. [S.l.]: Springer Science & Business Media, 2011. Cited 2 times on pages 28 and 29.

TAYLOR, R. H. et al. Medical robotics and computer-integrated surgery. In: *Springer handbook of robotics*. [S.l.]: Springer, 2016. p. 1657–1684. Cited on page 21.

TROFINO, A. Robust stability and domain of attraction of uncertain nonlinear systems. In: IEEE. *American Control Conference, 2000. Proceedings of the 2000*. [S.l.], 2000. v. 5, p. 3707–3711. Cited 2 times on pages 21 and 29.

TROFINO, A.; DEZUO, T. Lmi stability conditions for uncertain rational nonlinear systems. *International Journal of Robust and Nonlinear Control*, Wiley Online Library, v. 24, n. 18, p. 3124–3169, 2014. Cited 3 times on pages 21, 22, and 29.

WALSH, A.; FORBES, J. R. Modeling and control of flexible telescoping manipulators. *IEEE Transactions on Robotics*, v. 31, n. 4, p. 936–947, Aug 2015. ISSN 1552-3098. Cited on page 21.

WANGA XUZHI LAI, L. C.-H. D. M. W. Y. A quick control strategy based on hybrid intelligent optimization algorithm for planar n-link underactuated manipulators. 2017. Cited on page 21.

WU, Q. et al. Development and hybrid force/position control of a compliant rescue manipulator. *Mechatronics*, Elsevier, v. 46, p. 143–153, 2017. Cited on page 21.

ZHANG, H.; WANG, J. Vehicle lateral dynamics control through afs/dyc and robust gain-scheduling approach. *IEEE Transactions on Vehicular Technology*, IEEE, v. 65, n. 1, p. 489–494, 2015. Cited on page 74.

ZHANG, S. et al. A gain-scheduling approach to nonfragile h_∞fuzzy control subject to fading channels. *IEEE Transactions on Fuzzy Systems*, IEEE, v. 26, n. 1, p. 142–154, 2016. Cited on page 74.

ZHANG XUZHI LAI , Y. W. P. Quick and effective position control for planar n-link underactuated manipulators based on optimization algorithm. *Proceedings of the 37th Chinese Control Conference July 25-27, 2018, Wuhan, China*, 2018. Cited on page 21.

ZHANG XUZHI LAI , Y. W. P. Motion planning and adaptive neural sliding mode tracking control for positioning of uncertain planar underactuated manipulator. *Proceedings of the 37th Chinese Control Conference July 25-27, 2018, Wuhan, China*, 2019. Cited on page 21.

Pontifícia Universidade Católica do Rio Grande do Sul
Pró-Reitoria de Graduação
Av. Ipiranga, 6681 - Prédio 1 - 3º. andar
Porto Alegre - RS - Brasil
Fone: (51) 3320-3500 - Fax: (51) 3339-1564
E-mail: prograd@pucrs.br
Site: www.pucrs.br